Statistical model for diffusion-mediated recovery of dislocation and point-defect microstructure

I. Rovelli,[1,2,*] S. L. Dudarev,[2] and A. P. Sutton[1]

[1]*Department of Physics, Imperial College London, Exhibition Road, London SW7 2AZ, United Kingdom*

[2]*Culham Centre for Fusion Energy, UK Atomic Energy Authority, Abingdon, Oxfordshire OX14 3DB, United Kingdom*

(Received 12 February 2018; published 15 October 2018)

The evolution of the defect microstructure in materials at high temperature is dominated by diffusion-mediated interactions between dislocations, cavities, and surfaces. This gives rise to complex nonlinear couplings between interstitial and vacancy-type dislocation loops, cavities, and the field of diffusing vacancies that adiabatically follows the evolution of microstructure. In our previous work, we developed a nonlocal model for the climb of curved dislocations and the morphological evolution of cavities during postirradiation annealing of structural components in nuclear reactors. We now expand the formalism to include the treatment of population of very small defects and dislocation loops that are below the experimental detection limit. These are taken into account through a mean field approach coupled with an explicit real-space treatment of larger-scale discrete defect clusters. We find that randomly distributed small defects screen diffusive interactions between larger discrete clusters, renormalizing the free diffusion Green's functions and transforming them into Yukawa-type propagators. The evolution of the coupled system is modelled self-consistently, showing how the defect microstructure evolves through a nonmonotonic variation of the distribution of sizes of dislocation loops and cavities, treated as discrete real-space objects.

DOI: 10.1103/PhysRevE.98.043002

I. INTRODUCTION

In a metal at sufficiently high temperature, the evolution of its microstructure following irradiation is effected by diffusion. Point defects, predominantly vacancies, propagate between dislocations, cavities, grain boundaries, and surfaces, producing changes in their morphologies. The evolution rate of each microstructural defect is governed by the imbalance between the local chemical potential of vacancies in the atmosphere surrounding it, and the chemical potential of vacancies in the bulk. Each defect, acting as a sink or source of vacancies, introduces a perturbation of the vacancy concentration in the medium, varying as the inverse distance away from the defect. Therefore dislocations, vacancy clusters, and surfaces evolve through coupled diffusive interactions carried by the vacancy field, and the evolution of each one depends on the global defect microstructure.

A model for the evolution of an arbitrary configuration of vacancy clusters and dislocations at elevated temperatures is needed to predict changes of engineering properties of materials in nuclear fusion and fission reactors. High energy neutrons produced by nuclear reactions in fusion plasma, or emitted by fissile nuclear fuel, impact atoms in the structural components, generating vacancies and self-interstitials that aggregate to form prismatic vacancy and interstitial dislocation loops and cavities [1–5]. The accumulation of such defects degrades mechanical and thermal properties of materials. To design annealing protocols for the recovery of neutron irradiation damage [2], it is desirable to be able to predict the evolution of arbitrary populations of such defects in real space as a function of time and temperature postirradiation.

Molecular dynamics (MD) simulations have been instrumental in understanding the initial stage of defect production during irradiation due to short-lived (∼0.1–1 ps) collision cascades [6–8] and in characterizing the structure and mobility of small defect clusters [9]. However, the diffusion-driven evolution of interacting defect clusters involves time scales (μs to years) not accessible to MD simulations.

Two coarse-grained modeling frameworks have risen to prominence for the treatment of defect cluster evolution in irradiation conditions and during postirradiation annealing: mean field rate theory (MFRT) and kinetic Monte Carlo (KMC) [10,11].

In MFRT spatial distributions of defect clusters are represented by spatially independent or slowly spatially varying continuous size distribution functions (SDFs). The time evolution of SDFs are governed by coupled master equations involving defect generation rates (when considering processes during irradiation) and fluxes, in the defect size space, proportional to the rates of point-defect absorption and emission by various defect cluster types. Reaction rates are assumed to depend on the available populations of point defects, which are also dynamical quantities of the theory, evolving according to the average effective sink strength of defect clusters and other microstructural features [12]. While it is possible to introduce a degree of spatial information, for instance by considering multiple subsystems with different but co-evolving cluster densities, MFRT models fundamentally employ spatially averaged descriptions of defect cluster distributions and hence they are unable to treat real-space diffusion-driven processes like the correlated diffusion-mediated evolution of dislocation loops.

*Corresponding author: ir1014@ic.ac.uk

KMC models treat defect clusters and individual point defects as discrete objects with explicit positions in the simulation cell, while their time evolution is governed stochastically instead of deterministically. A set of possible transition *events* is specified for the various classes of objects, such as migration, emission or aggregation of point defects from or to clusters, and vacancy-interstitial annihilation. At each time step, an event is randomly chosen with probability proportional to the Arrhenius factor with the relevant energy barrier for the reaction [13]. A particular object able to undergo the reaction is then randomly selected, the state of the system is updated accordingly, and time is advanced by an amount inversely proportional to the total reaction rate. The computational cost of KMC is generally considerably higher than MFRT, therefore simulations are limited to smaller cell sizes, typically of the order of a few hundred nm, and relatively low [<1 displacements per atom (dpa)] doses [14]. The main limitation of KMC models is that the method requires choosing the objects and reaction rules at the start of the simulation. It is possible to model the evolution of populations of dislocation loops and vacancy clusters as long as the defect structures formed as a result of reactions between the existing objects belong to the same class of objects, for which the rules of evolution are defined. For example, if the objects defined in a KMC simulation are circular prismatic dislocation loops, then a simulation is unable to predict the formation of dislocation loops with noncircular shapes or the formation of a dislocation network, such as those often observed in experiment. The number of individual defects that a KMC simulation can handle is also limited, as the total reaction rate increases in proportion to the total number of objects in a simulation cell. This reduces the simulation time step and makes it difficult to treat evolution in the high temperature limit where the concentration of mobile vacancies is high.

In an earlier paper [15] we presented a formalism that extends the nonlocal dislocation climb model of Gu *et al.* [16] to simulate the evolution of discrete dislocation loops and vacancy clusters in a finite medium, at high temperatures and in real space. One of the motivations for developing a real-space model, in contrast to a spatially averaged MFRT approach, is that the sizes of clusters of vacancies or self-interstitials produced by neutron irradiation appear to obey a power-law probability distribution [6,17] of the form $f(n) \sim n^{-s}$, with n the number of self-interstitials or vacancies in the cluster. For $s < 2$, corresponding to experimental observations [17], the average size of a defect cluster is not defined, and so a representative cluster size of a rate theory model remains undefined. A real-space model can also treat local variations in the number density of clusters, for instance those arising from depleted zones [18] at grain boundaries and free surfaces.

The nonhomogeneous spatial arrangement of defects and dislocation segments in irradiated samples is clearly evident in transmission electron microscopy (TEM) images of ion irradiated tungsten foil shown in Fig. 1. Furthermore, the *in situ* TEM observations of dynamics of postirradiation annealing have highlighted a strong dependence of evolution of individual defect clusters on the local defect distribution in their local environment [2].

In principle, KMC models might allow, subject to the limitations noted above, the simulation of arbitrary spatial distributions of defect clusters. However, the computational cost of our real-space model is many orders of magnitude lower, as individual point defects are not explicitly taken into account as stochastic discrete entities. As a result, we are able to treat larger simulation cells, higher densities of defect clusters, and considerably longer time scales. In addition, our model does not preclude the treatment of arbitrary dislocation structures outside of circular loops, and in principle can be integrated in discrete dislocation dynamics (DDD) models.

FIG. 1. TEM snapshot of *in situ* annealing of ion-irradiated tungsten (2-MeV W^+ ions, 500 °C, 10^{14} W^+/cm^2) at 700 °C. Adapted with permission from [2].

It is likely that the experimentally determined number of the smallest defect clusters is always underestimated owing to detection limits of the instrumentation. The sizes of experimentally observed defect clusters is usually assumed to obey a Gaussian-like distribution. Such a distribution can be understood as a product of the true distribution with a sigmoid function representing the instrumental sensitivity, as sketched in Fig. 2. Therefore, experimental data on radiation induced defect clusters is generally incomplete and the number density of the smallest "invisible" defect clusters can be much greater than the observed population, as recently noted by Liu *et al.* [19].

It would be useful, therefore, to include a statistical description of the unknown small-size cluster population, introducing an effective mean field which evolves self-consistently with the observable cluster population. This approach would provide an efficient way to investigate the effect of invisible clusters on the distribution of sizes of visible clusters. It turns out that the mean field is governed by only a few low-order moments of the size distribution of visible clusters, which can be determined by the experimentally measured evolution of the observable population. In this paper we present a hybrid model that couples the evolution of an experimentally visible, discrete population of defect clusters in real space with a mean field, representing the experimentally invisible clusters.

In Sec. II we estimate the expected time scales for the evaporation of nanometric cavities as a function of temperature in W, Fe, and Be. In Sec. III we introduce the mean field formulation by averaging the positions and sizes of the small

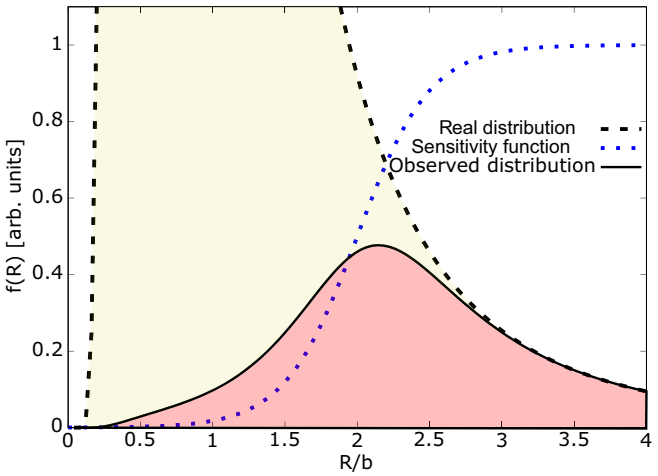

FIG. 2. Qualitative explanation of the observed Gaussian-like size distribution of defect clusters in neutron irradiated tungsten. The dashed black line represents the true, power-law like, size distribution. The dotted blue line represents the experimental sensitivity function plotted as a function of cluster size. The solid black line is the observed distribution, given by the product of the true distribution and the sensitivity function. The red shaded area is proportional to the number density of the observed clusters, while the yellow shaded area is proportional to the number density of mostly "invisible" clusters.

clusters, using a technique developed in scattering theory by Edwards [20]. In this way we obtain a general expression, Eq. (32), for the coarse-grained vacancy concentration in the presence of an arbitrary distribution of small clusters.

In Appendix B we present a perturbative approach that expands Eq. (32) in terms of an increasing number of scattering events, deriving an analog of the self-energy expansion for condensed matter systems. In the case of homogeneous and uncorrelated distributions, we provide closed form expressions for the self-energy up to the third order terms in Eq. (B11).

By considering the first order approximation to the effective self-energy, we show that the effective Green's function governing the interaction between the observable clusters takes the form of a Yukawa propagator, Eq. (40). Thus, we show that diffusive interactions mediated by vacancies between larger clusters are screened by the mean field of small clusters. The formalism has similarities to the *diffusion screening theory*, originally due to Marqusee and Ross [21] and further developed by other authors [22–26], which addresses the issue of divergences in Ostwald ripening theories for finite volume fractions of particles. In *diffusion screening theory* the usual Laplacian diffusive interactions are screened as a result of coarse-graining second phase particles, which is analogous to our mean field treatment of invisible defect clusters. This procedure enables us in Eq. (43) to provide a closed form expression for the vacancy field where only observable clusters are treated explicitly.

The rates of growth of cavities can be calculated self-consistently in the same manner as in our previous model [15] by evaluating the vacancy field at the cluster positions with defined boundary conditions. We couple the evolution of the mean field with large clusters via Eqs. (46) and (49).

The theory is developed for an infinite medium. However, the majority of experimental data on radiation-induced defect clusters has so far been obtained using thin film samples. In Sec. IV we present an extension of the theory to a thin film infinitely extended in the lateral direction, making use of a variant of Ewald summation developed for Yukawa potentials [27]. In Sec. V we briefly present a mean field treatment of all defect clusters. Finally, in Sec. VI we present numerical simulations to illustrate applications of the theory to the evolution of distributions of cluster sizes in irradiated thin films of W, Be, and Fe.

II. PRELIMINARY ESTIMATE OF GOVERNING TIME SCALES

An estimate of the time scale required for the complete evaporation of a nanometric defect cluster can be obtained by considering the isolated cluster in a vacancy atmosphere in local thermodynamic equilibrium. In general, the characteristic time scales for vacancy equilibration are much shorter than the time scales for significant morphological changes of defect clusters. As a consequence, the usual approach in modeling dislocation-climb and diffusion-mediated microstructural evolution consists in assuming instantaneous equilibration of the vacancy field with respect to the defect cluster morphology [28–32]. We have discussed the validity of this assumption quantitatively in our previous work [15]. In particular, in the case of nanometric dislocation loops or cavities, transient effects due to vacancy equilibration become important only on a spatial scale roughly 100 times larger than the defect cluster size. At such distances, however, perturbations of the vacancy field arising from the cluster evolution are already negligible due to the $1/r$ dependence of the diffusion propagator.

Consider an isolated spherical cavity of radius R. Assuming an adiabatic evolution of the vacancy concentration with respect to the cavity, we have

$$\frac{dR}{dt} = \frac{D_v}{R}[c_0 - c_\Sigma(R)], \tag{1}$$

where c_Σ is the local vacancy concentration at the cavity surface and c_0 is the equilibrium vacancy concentration per atomic site, given by $c_0 = \exp(-E_v/k_BT)$ where E_v is the vacancy formation energy. $c_\Sigma(R)$ is determined by the condition of local equilibrium, i.e., there is no change in free energy if vacancies attach to or detach from the cavity, which leads to the Gibbs-Thomson expression:

$$c_\Sigma(R) = c_0 \exp\left(\frac{2\gamma\Omega}{Rk_BT}\right), \tag{2}$$

where γ is the cavity surface energy per unit area and Ω is the atomic volume. Therefore, if we consider a system of cavities of average radius $\bar{R}$ evolving adiabatically with a vacancy field in local thermodynamic equilibrium we can estimate the characteristic time scale for cavity evaporation as follows:

$$\tau_e = \frac{\bar{R}^2}{D_v[c_0 - c_\Sigma(\bar{R})]} = \frac{\bar{R}^2}{D_v^0}\exp\left(\frac{E_v + E_m}{k_BT}\right) \times \left[\exp\left(\frac{2\gamma\Omega}{\bar{R}k_BT}\right) - 1\right]^{-1}, \tag{3}$$

TABLE I. Material parameters used in the present work. Parameters for Be are averages of basal and nonbasal values. 1 eV/nm^2 ∼ 0.16 J/m^2.

Material	γ (eV/nm^2)	μ (GPa)	ν	b (nm)	Ω (nm^3)	$E_{\rm v}$ (eV)	$E_{\rm m}$ (eV)	$D_{\rm v}^0$ (nm^2/s)]
W	20.4[a]	161[b]	0.28[b]	0.27[b]	0.016[b]	3.56[c]	1.78[c]	4.0×10^{12}[d]
Fe	15.3[a]	82[b]	0.29[b]	0.29[b]	0.012[b]	2.07[c]	0.65[c]	2.8×10^{14}[e]
Be	12.5[a]	132[b]	0.03[b]	0.18[b]	0.008[b]	0.95[c]	0.81[c]	5.7×10^{13}[f]

[a]Reference [34].
[b]Reference [35].
[c]Reference [36].
[d]Reference [37].
[e]Reference [38].
[f]Reference [39].

where E_v and E_m are respectively the vacancy formation and migration energies, and D_v^0 is the pre-exponential factor of the diffusion coefficient.

In a similar way, we can estimate the characteristic time scale of dislocation loop evaporation by considering the rate of change of the radius of an isolated circular prismatic loop due to nonconservative dislocation climb [16]:

$$\frac{dR}{dt} = \pm \frac{2\pi D_v}{b_e \ln(8R/r_d)}[c_0 - c_\Delta(R)], \tag{4}$$

where the plus or minus sign denotes respectively the case of a vacancy or interstitial loop, b_e is the edge (out of plane) component of the dislocation Burgers vector, r_d is the radius of the dislocation core, and c_Δ is the vacancy concentration infinitesimally close to the dislocation line. The assumption of local equilibrium between the dislocation loop and the vacancy field surrounding it leads to the following relation:

$$c_\Delta(R) = c_0 \exp\left[-\frac{f_{\rm cl}(R)\Omega}{b_e k_B T}\right], \tag{5}$$

where, for a circular prismatic loop [33],

$$f_{\rm cl}(R) = \mp \frac{\mu b_e^2}{4\pi(1-\nu)R}\left[\ln\left(\frac{8R}{r_d}\right) - 1\right] \tag{6}$$

is the climb force per unit length of the dislocation,[1] ν is Poisson's ratio and μ is the shear modulus, and the minus or plus signs distinguish between vacancy type and interstitial type, respectively. We can therefore estimate the characteristic time scale for the evaporation of a dislocation loop of radius $\bar{R}$ as

$$\tau_{\rm e} = \pm \frac{b_e \bar{R} \ln(8\bar{R}/r_d)}{2\pi D_v^0} \exp\left(\frac{E_{\rm v} + E_{\rm m}}{k_B T}\right) \times \left\{ \exp\left[\pm \frac{\mu \Omega b_e}{4\pi(1-\nu)k_B T}\left(\ln\left(\frac{8\bar{R}}{r_d}\right) - 1\right)\right] - 1\right\}^{-1}. \tag{7}$$

[1]In this treatment we neglect the additional contributions to the climb force due to stresses imposed on the system as a whole or arising from other loops. This is a good approximation because we are considering very small loops (a few nanometers wide) for which the self-interaction stress dominates. We have defined the climb force as the projection of the Peach-Koehler force in the direction of the cross product between the dislocation line direction and the Burgers vector. Therefore, the climb force acting on a vacancy loop is the negative of that acting on an interstitial loop.

The parameters used for the investigated materials throughout the present work are given in Table I.

We applied Eq. (3) to bcc iron, tungsten, and beryllium, which are candidate materials for nuclear fusion engineering applications, with $\bar{R} = 1$ nm, which is within the range of experimentally observed sizes of radiation-induced cavities and dislocation loops. The computed $\tau_{\rm e}$ are plotted in Fig. 3 as a function of the homologous temperature $T/T_{\rm m}$, where $T_{\rm m}$ is the melting point. It is evident that $\tau_{\rm e}$ can vary over many orders of magnitude: from milliseconds to years, depending on temperature and material properties.

We note that although W shares the same crystal structure as Fe in Fig. 3, there is a systematic difference of at least one order of magnitude in the time scale τ_e for cavities and dislocation loops, even after scaling the temperature to the relevant melting point.

In Fig. 4 we plot the dependence of the relative change of predicted time scales $\Delta\tau_e/\tau_e$ for cavity evaporation on relative changes in the activation energy for diffusion by vacancy mechanism $\Delta E_a/E_a$, where $E_a = E_{\rm v} + E_{\rm m}$, and relative changes in the surface energy $\Delta\gamma/\gamma$, of up to ±10%, at $T = 0.4\,T_{\rm m}$. In Fig. 4(a) we see that an overestimation of

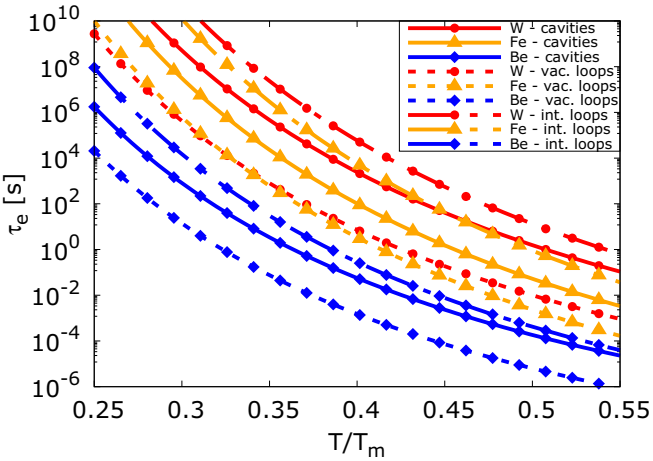

FIG. 3. Estimated time scales $\tau_{\rm e}$ for the evaporation and annihilation of ∼1 nm cavities (solid lines), vacancy dislocation loops (dashed lines), and interstitial dislocation loops (solid-dashed lines) in W (red, circles), Fe (yellow, triangles), and Be (blue, diamonds), as functions of homologous temperature $T/T_{\rm m}$.

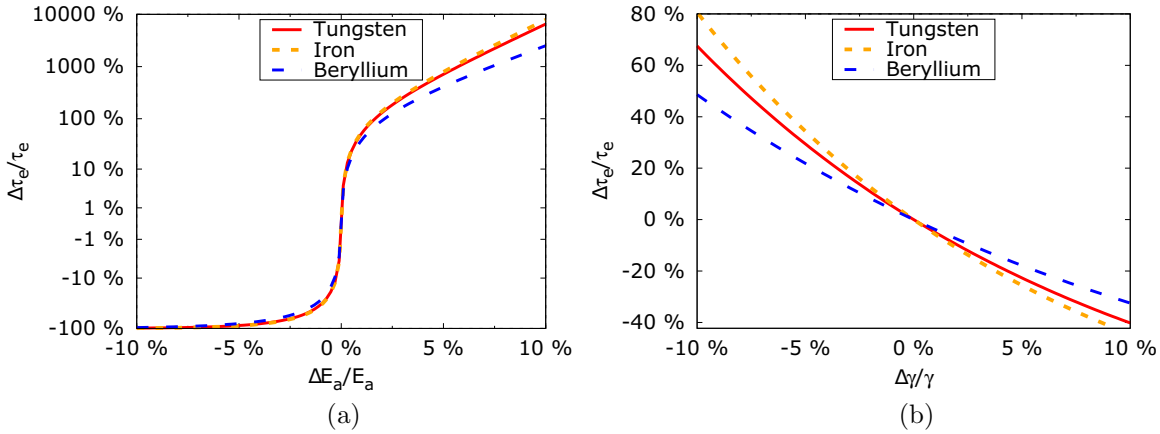

FIG. 4. Relative change of the estimated time scale τ_e for cavity evaporation at $T/T_m = 0.4$ with respect to small deviations of activation energy for diffusion by vacancy mechanism $E_a = E_v + E_m$ (a) and surface energy γ (b). In plot (a) the scale of the y axis is linear between -1% and 1% and logarithmic elsewhere.

E_a by just $\sim 2\%$ leads to a relative error of at least 100% for τ_e in all three materials. This extreme sensitivity, arising from the exponential dependence of τ_e on the formation and migration energies of vacancies should be kept in mind when attempting to compare experimentally observed time scales with theoretical estimates. Activation energies for diffusion can be affected by a number of factors which may not be under experimental control, such as the presence of bound impurity-vacancy complexes, or a dependence of the entropy of activation on temperature, which may become significant at higher temperatures [40]. The sensitivity to errors in the assumed surface energy is less extreme, but also a source of uncertainty because the surface energy per unit area of clusters with radius as small as 1 nm or less may differ significantly from the surface energies per unit area of larger clusters.

III. DEFINITION OF THE MEAN FIELD FORMALISM

A. Adiabatic vacancy field in the presence of a small defect cluster

Consider an infinite crystal containing a circular prismatic dislocation loop of radius R, with its center at the origin and lying in the x-y plane. The loop may be of vacancy or interstitial character. Since the loop lies in the x-y plane, the component b_e of the Burgers vector normal to the loop (i.e., along the z axis) remains constant at all points around the loop. Let $c(\mathbf{x})$ be the vacancy concentration per atomic site, i.e., $c(\mathbf{x})$ is the (dimensionless) probability of finding a vacancy at a lattice site at $\mathbf{x}$, and let us assume that vacancies are the only mobile point defects. If we further assume that the evolution of the vacancy field is adiabatic with respect to changes in the loop configuration,[2] we can write [16] the following equation:

$$c(\mathbf{x}) = -\frac{b_e}{4\pi D_v} \oint_\Gamma \frac{v_{\rm cl}(\mathbf{x}')}{|\mathbf{x}-\mathbf{x}'|} dl' + c_\infty, \tag{8}$$

where Γ denotes the dislocation line, $v_{\rm cl}(\mathbf{x})$ is the dislocation climb velocity, and c_∞ is the vacancy concentration at infinity. We define $v_{\rm cl}(\mathbf{x})$ as the projection of the velocity of a point on Γ along the vector defined by the cross product between the tangent vector to the dislocation line at $\mathbf{x}$ and the Burgers vector.

Throughout this paper we adhere to the definition of the Burgers vector used by Hirth and Lothe [33], i.e., given a circular path C, drawn around a dislocation line according to the right hand rule with respect to the dislocation line direction, the Burgers vector $\mathbf{b}$ is defined as

$$\mathbf{b} = \oint_C \frac{\partial \mathbf{u}}{\partial l} dl, \tag{9}$$

where $\mathbf{u}$ is the displacement field arising from the dislocation. This implies that the cross product between the tangent vector to the dislocation line and the Burgers vector points inward toward the center of a prismatic interstitial loop, and outward away from the center of a prismatic vacancy loop. We warn the reader that the opposite convention is used by Landau [41], Trinkaus [42], and others, where the direction of the Burgers vector is reversed with respect to the direction of the dislocation line. We also define the normal direction $\hat{\mathbf{n}}$ to the surface enclosed by a dislocation loop according to the right hand rule with respect to the dislocation line direction, so that $\mathbf{b}$ and $\hat{\mathbf{n}}$ are parallel for a prismatic vacancy loop and antiparallel for a prismatic interstitial loop.

We point out that Eq. (8) is the scalar form of a general vector equation (see Appendix A for details):

$$\begin{aligned} c(\mathbf{x}) &= -\frac{1}{4\pi D_v} \oint_\Gamma \frac{\mathbf{v}(\mathbf{x}')}{|\mathbf{x}-\mathbf{x}'|} \cdot (d\mathbf{l}' \times \mathbf{b}) + c_\infty \\ &= \oint_\Gamma G(|\mathbf{x}-\mathbf{x}'|)\mathbf{v}(\mathbf{x}') \cdot (d\mathbf{l}' \times \mathbf{b}) + c_\infty, \end{aligned} \tag{10}$$

where $G(|\mathbf{x}|) = -1/4\pi D_v|\mathbf{x}|$ is the free space Green's function of the steady-state diffusion equation, $D_v \nabla^2 G(|\mathbf{x}|) = \delta(\mathbf{x})$, $\mathbf{v}(\mathbf{x}')$ is the vector velocity of a point $\mathbf{x}' \in \Gamma$, $\mathbf{b}$ is the Burgers vector of the dislocation loop, and the differential $d\mathbf{l}'$ is tangential to the dislocation line at $\mathbf{x}'$.

[2]This assumption implies that local equilibrium exists between each dislocation segment and the surrounding vacancy field. For quantitative bounds on this assumption see [15].

By evaluating Eq. (8) on Γ and using Eq. (5) we can self-consistently find an analytical solution for $v_{\rm cl}(\mathbf{x})$, leading to a closed-form expression for the vacancy concentration in the medium:

$$c(\mathbf{x}) = c_\infty - \frac{1}{2\ln(8R/r_d)} \oint_\Gamma \frac{1}{|\mathbf{x}-\mathbf{x}'|}[c_\infty - c_\Delta(R)]dl'. \quad (11)$$

Let r denote the distance between $\mathbf{x}$ and the center of the dislocation loop and let $\phi = \cos^{-1}(z/r)$, where z is the component of $\mathbf{x}$ out of the x-y plane. In the limit of $r \gg R$ we can expand the above integrand in powers of R/r to obtain

$$c(r,\phi) = c_\infty - [c_\infty - c_\Delta(R)]\frac{\pi}{\ln(8R/r_d)}\left(\frac{R}{r}\right) \times \left[1+\frac{1}{2}\left(\frac{R}{r}\right)^2\left(\frac{3\sin^2\phi}{2}-1\right)+O\left(\frac{R}{r}\right)^3\right], \quad (12)$$

where $\phi = \cos^{-1}(z/r)$, and z is the component of $\mathbf{x}$ out of the x-y plane. The above expression shows that to second order in R/r, a dislocation loop, or in fact any defect cluster, can be treated as a spherically symmetric vacancy source or sink.

On the other hand, the vacancy field sufficiently far from an isolated spherical cavity at the origin can be *exactly* interpreted as originating from a pointlike source. Indeed, at all $r > R$, Newton's shell theorem shows that the vacancy concentration is a function of the distance to the center of the cavity r, and is given by [15,43]

$$c(r) = c_\infty - [c_\infty - c_\Sigma(R)]\left(\frac{R}{r}\right). \quad (13)$$

We note that the above expressions are examples of a more general equation that admits a clear physical interpretation. The vacancy field at large distances from *any* point-defect cluster situated at the origin, which can be approximated as an isotropic pointlike source, is characterized by the rate of change of the volume of the cluster[3] $\mathcal{V}$:

$$c(\mathbf{x}) = c_\infty - \frac{d\mathcal{V}}{dt}G(|\mathbf{x}|). \quad (14)$$

This statement can be proven straightforwardly for a spherical cavity, where

$$\frac{d\mathcal{V}_{\rm cav}}{dt} = \frac{d}{dt}\left(-\frac{4\pi}{3}R^3\right) = -4\pi R^2\frac{dR}{dt} = -4\pi D_v R[c_\infty - c_\Sigma(R)], \quad (15)$$

which, upon substitution in Eq. (14), leads to Eq. (13).

For a prismatic dislocation loop we prove in Appendix A that

$$\frac{d\mathcal{V}_{\rm loop}}{dt} = -\oint_\Gamma \mathbf{v}(\mathbf{x}')\cdot(d\mathbf{l}'\times\mathbf{b}) = -\oint_\Gamma \mathbf{b}\cdot(\mathbf{v}(\mathbf{x}')\times d\mathbf{l}') = -\oint_\Gamma v_{\rm cl}(\mathbf{x}')b_e(\mathbf{x}')dl', \quad (16)$$

which, assuming constant $v_{\rm cl}(\mathbf{x}')$ and $b_e(\mathbf{x}')$ over Γ, becomes

$$\frac{d\mathcal{V}_{\rm loop}}{dt} = -2\pi R v_{\rm cl} b_e = -\frac{4\pi^2 R D_v}{\ln(8R/r_d)}[c_\infty - c_\Delta(R)], \quad (17)$$

giving the leading order term of Eq. (12) upon substitution in Eq. (14).

To simplify the presentation, we will consider only interstitial dislocation loops forming the invisible cluster population. This assumption is justified by the fact that the energy gain associated with the formation of a vacancy cluster is smaller than that of an interstitial cluster [44,45], and in general a vacancy cluster has to be of appreciable size to remain stable at a finite temperature [46].

Also, in general c_∞ should depend on time, following adiabatically the evolution of all the clusters in the system. However, in a real finite system c_∞ is governed at equilibrium by the surface energy and geometry of its external boundaries (free surfaces, grain boundaries), and can thus be considered constant in time for practical applications, provided that the morphology of external boundaries does not change appreciably during the evolution.

B. Representing the invisible dislocation loops by a mean field fully coupled to the visible clusters

Consider N cavities and n interstitial prismatic loops in an infinite medium. The cavities are sufficiently large and they are visible experimentally, but the prismatic loops are too small to be detected. In the following the evolution of the cavities will be considered explicitly as discrete objects, but the evolution of the loops will be treated through a mean field. The evolution of the cavities and the mean field will be fully coupled.

Let $c_b(\mathbf{x})$ be the vacancy concentration field obtained by considering only the cavities. It is given by the equation

$$D_v\nabla^2 c_b(\mathbf{x}) = \Omega J_n(\mathbf{x})\sum_{i=1}^{N}\delta[\Sigma_i(t)], \quad (18)$$

where $\Sigma_i(t)$ denotes the surface of the ith cavity at time t, and J_n is the vacancy current normal to a cavity surface, where the normal direction is considered pointing from the bulk towards the center of the cavity, i.e., $J_n(\mathbf{x}) > 0$ if vacancies are entering the cavity at $\mathbf{x}$. $\delta(\Sigma)$ represents a delta function evaluated on a surface, defined as

$$\int_V \varphi(\mathbf{x})\delta(\Sigma)dV = \int_\Sigma \varphi(\mathbf{x})dS, \quad (19)$$

where $\varphi(\mathbf{x})$ is an arbitrary trial function and V is an arbitrary volume containing the surface Σ.

Consider the invisible interstitial loops. Let $\mathbf{x}_i$ and R_i denote respectively the center and the radius of the ith loop. To simplify the notation and make clear the parametric dependencies of the various functions, we define the following sets:

$$\begin{aligned}\mathcal{X} &= \{\mathbf{x}_i : i = 1,\dots,n\},\\ \mathcal{R} &= \{R_i : i = 1,\dots,n\},\\ \mathcal{X}_{[i]} &= \{\mathbf{x}_j : j = 1,\dots,n;\ j\neq i\},\\ \mathcal{R}_{[i]} &= \{R_j : j = 1,\dots,n;\ j\neq i\},\end{aligned} \quad (20)$$

[3]With the caveat that $\mathcal{V}$ is negative for vacancy clusters or voids because their growth reduces the overall vacancy concentration in solution, and positive for interstitial clusters because their growth increases the overall vacancy concentration in solution assuming there are no free interstitial atoms.

and we introduce the shorthand notations

$$d\mathcal{X} = \prod_{i=1}^{n} d\mathbf{x}_i, \quad d\mathcal{R} = \prod_{i=1}^{n} dR_i,$$
$$d\mathcal{X}_{[i]} = \prod_{j\neq i}^{n} d\mathbf{x}_j, \quad d\mathcal{R}_{[i]} = \prod_{j\neq i}^{n} dR_i. \tag{21}$$

The total vacancy field obtained by also considering the effect of the n dislocation loops can then be expressed as [20]

$$\begin{aligned} c(\mathbf{x};\mathcal{X},\mathcal{R}) &= c_b(\mathbf{x}) - \sum_{i=1}^{n} \frac{d\mathcal{V}_i}{dt} G(|\mathbf{x}-\mathbf{x}_i|) \\ &= c_b(\mathbf{x}) + \sum_{i=1}^{n} \xi_\Delta(R_i) G(|\mathbf{x}-\mathbf{x}_i|) \\ &\quad \times [c_{[i]}(\mathbf{x}_i;\mathcal{X},\mathcal{R}) - c_\Delta(R_i)], \end{aligned} \tag{22}$$

where $\xi_\Delta(R) = 4\pi^2 R D_v/\ln(8R/r_d)$. The vacancy field obtained by omitting the contribution arising from the ith loop is $c_{[i]}(\mathbf{x};\mathcal{X},\mathcal{R})$, and it is defined by the self-consistent condition:

$$\begin{aligned} c_{[i]}(\mathbf{x};\mathcal{X},\mathcal{R}) &= c_b(\mathbf{x}) + \sum_{j\neq i}^{n} \xi_\Delta(R_j) G(|\mathbf{x}-\mathbf{x}_j|) \\ &\quad \times [c_{[j]}(\mathbf{x}_j;\mathcal{X},\mathcal{R}) - c_\Delta(R_j)]. \end{aligned} \tag{23}$$

We define the probability of finding the n dislocation loops in the n volume elements $(\mathbf{x}_1 + d\mathbf{x}_1, \ldots, \mathbf{x}_n + d\mathbf{x}_n)$, and with loop radii in the ranges $(R_1 + dR_1, \ldots, R_n + dR_n)$, as

$$p(\mathcal{X},\mathcal{R}) d\mathcal{X} d\mathcal{R}. \tag{24}$$

The average of Eq. (22) with respect to the positions and radii of each loop can then be expressed as

$$\begin{aligned} \bar{c}(\mathbf{x}) &= \int c(\mathbf{x};\mathcal{X},\mathcal{R}) p(\mathcal{X},\mathcal{R}) d\mathcal{X} d\mathcal{R} \\ &= c_b(\mathbf{x}) + \sum_{i=1}^{n} \int \big[S^i_{\rm nl}(\mathbf{x};\mathcal{X},\mathcal{R}) \\ &\quad - S_{\rm l}(\mathbf{x};\mathbf{x}_i,R_i)\big] p(\mathcal{X},\mathcal{R}) d\mathcal{X} d\mathcal{R}, \end{aligned} \tag{25}$$

where $S^i_{\rm nl}(\mathbf{x};\mathcal{X},\mathcal{R})$ and $S_{\rm l}(\mathbf{x};\mathbf{x}_i,R_i)$ are respectively the nonlocal and local contributions of the ith loop to the total concentration field, defined as

$$\begin{aligned} S^i_{\rm nl}(\mathbf{x};\mathcal{X},\mathcal{R}) &= \xi_\Delta(R_i) G(|\mathbf{x}-\mathbf{x}_i|) c_{[i]}(\mathbf{x}_i;\mathcal{X},\mathcal{R}), \\ S_{\rm l}(\mathbf{x};\mathbf{x}_i,R_i) &= \xi_\Delta(R_i) G(|\mathbf{x}-\mathbf{x}_i|) c_\Delta(R_i). \end{aligned} \tag{26}$$

$S_{\rm l}$ is the perturbation to the vacancy field in the neighborhood of the ith loop arising from the condition of local thermodynamic equilibrium. The nonlocal term $S^i_{\rm nl}$ describes the contribution to the vacancy field near loop i from all the other loops in the system.

By introducing the one-loop probability density function,

$$p_1(\mathbf{x}_i,R_i) = \int p(\mathcal{X},\mathcal{R}) d\mathcal{X}_{[i]} d\mathcal{R}_{[i]}, \tag{27}$$

we can express the average of the local contribution as

$$\bar{S}_{\rm l}(\mathbf{x}) = \int S_{\rm l}(\mathbf{x};\mathbf{x}_i,R_i) p_1(\mathbf{x}_i,R_i) d\mathbf{x}_i dR_i, \tag{28}$$

which can be readily calculated without any knowledge of correlations in the positions or radii of different loops, requiring only the single loop spatial and size distribution $p_1(\mathbf{x},R)$.

We now average the nonlocal contribution. Let us define the conditional probability density $p(\mathbf{x}_i,R_i|\mathcal{X}_{[i]},\mathcal{R}_{[i]})$ by the relation

$$p_1(\mathbf{x}_i,R_i)\, p(\mathbf{x}_i,R_i|\mathcal{X}_{[i]},\mathcal{R}_{[i]}) = p(\mathcal{X},\mathcal{R}) \tag{29}$$

and the effective averaged vacancy field experienced by the ith loop as

$$\bar{c}^{\rm eff}_{[i]}(\mathbf{x};\mathbf{x}_i,R_i) = \int c_{[i]}(\mathbf{x};\mathcal{X},\mathcal{R}) p(\mathbf{x}_i,R_i|\mathcal{X}_{[i]},\mathcal{R}_{[i]}) d\mathcal{X}_{[i]} d\mathcal{R}_{[i]}. \tag{30}$$

By employing these definitions, we may write the average of the nonlocal contribution as

$$\bar{S}_{\rm nl}(\mathbf{x}) = \int \xi_\Delta(R_i) G(|\mathbf{x}-\mathbf{x}_i|) \bar{c}^{\rm eff}_{[i]}(\mathbf{x};\mathbf{x}_i,R_i)\, p_1(\mathbf{x}_i,R_i) d\mathbf{x}_i dR_i. \tag{31}$$

In summary, the governing equation for the vacancy concentration, averaged over all possible positions and radii of the invisible interstitial loops, is given by

$$\begin{aligned} \bar{c}(\mathbf{x}) &= c_b(\mathbf{x}) + n \int \xi_\Delta(R_i) G(|\mathbf{x}-\mathbf{x}_i|)\, p(\mathbf{x}_i;R_i) \\ &\quad \times \big[\bar{c}^{\rm eff}_{[i]}(\mathbf{x};\mathbf{x}_i,R_i) - c_\Delta(R_i)\big] d\mathbf{x}_i dR_i. \end{aligned} \tag{32}$$

The integral in this equation is the mean field of the invisible loops in which the visible clusters sit. Information about correlations between the positions and sizes of the invisible loops is contained in the effective field $\bar{c}^{\rm eff}_{[i]}$.

C. The simplest approximation of the field $\bar{c}^{\rm eff}_{[i]}$ of Eq. (30) and screening

A formal expansion of the effective field defined in Eq. (30) is derived in Appendix B, which provides the theoretical foundation to treat correlations between the positions of the invisible loops to arbitrary degrees of accuracy. In this section we consider the simplest approximation, which is to neglect all these correlations. We may then characterize the loops entirely through the size distribution function $f(R)$, which is related to the single-loop probability density function as follows:

$$p_1(\mathbf{x},R) = n^{-1} f(R). \tag{33}$$

In the above equation, $f(R)dR$ is the number of dislocation loops per unit volume with radii between R and $R+dR$.

Provided the concentration of invisible loops is sufficiently large, it is reasonable to assume that the average vacancy field seen by dislocation loops is equal to the configuration averaged field, i.e., $\bar{c}(\mathbf{x}) \approx \bar{c}^{\rm eff}_{[i]}$. In these approximations Eq. (32) for the configuration-averaged concentration takes on the form

$$\begin{aligned} \bar{c}(\mathbf{x}) &= c_b(\mathbf{x}) + \int dV' G(|\mathbf{x}-\mathbf{x}'|) \int_b^\infty \xi_\Delta(R) f(R) \\ &\quad \times [\bar{c}(\mathbf{x}') - c_\Delta(R)] dR, \end{aligned} \tag{34}$$

where the Burgers vector b acts as a lower bound on the possible dislocation loop size. We now define the averages:

$$\overline{\xi_\Delta} = \int_b^\infty dR f(R)\xi_\Delta(R),$$
$$\overline{\xi_\Delta c_\Delta} = \int_b^\infty dR f(R)\xi_\Delta(R)c_\Delta(R), \tag{35}$$

where both have the dimensions of inverse time. Equation (34) then becomes

$$\bar{c}(\mathbf{x}) = c_b(\mathbf{x}) + \int dV' G(|\mathbf{x}-\mathbf{x}'|)[\overline{\xi_\Delta}\bar{c}(\mathbf{x}') - \overline{\xi_\Delta c_\Delta}]. \tag{36}$$

We apply the operator $D_v\nabla^2$ to both sides of Eq. (36), obtaining

$$D_v\nabla^2\bar{c}(\mathbf{x}) = D_v\nabla^2 c_b(\mathbf{x}) + \int dV' \delta(\mathbf{x}-\mathbf{x}')[\overline{\xi_\Delta}\bar{c}(\mathbf{x}') - \overline{\xi_\Delta c_\Delta}], \tag{37}$$

which, along with Eq. (18), can be reorganized as

$$(D_v\nabla^2 - \overline{\xi_\Delta})\bar{c}(\mathbf{x}) = \Omega J_n(\mathbf{x}) \sum_{i=1}^N \delta[\Sigma_i(t)] - \overline{\xi_\Delta c_\Delta}. \tag{38}$$

Equation (38) has the mathematical structure of an inhomogeneous Debye-Hückel equation.

The Yukawa Green's function, $G_Y(|\mathbf{x}-\mathbf{x}'|;\overline{\xi_\Delta})$, is defined by the equation

$$(D_v\nabla^2 - \overline{\xi_\Delta})G_Y(|\mathbf{x}-\mathbf{x}'|;\overline{\xi_\Delta}) = \delta(\mathbf{x}-\mathbf{x}'), \tag{39}$$

for which the solution is

$$G_Y(|\mathbf{x}-\mathbf{x}'|;\overline{\xi_\Delta}) = -\frac{\exp\{-\sqrt{\overline{\xi_\Delta}/D_v}\,|\mathbf{x}-\mathbf{x}'|\}}{4\pi D_v|\mathbf{x}-\mathbf{x}'|}. \tag{40}$$

Thus, the diffusive interaction between cavities in Eq. (37) is *screened* by the mean field of the dislocation loops. The screening coefficient, $\sqrt{D_v/\xi_\Delta}$, limits the range of direct diffusional interaction between cavities.

In this continuum treatment, once the effect of the loop population is replaced by a mean field, the medium between the cavities becomes a net adsorber for vacancies. This reflects the reality at the atomic scale where the mean free path of propagating vacancies is reduced by the presence of distributed sinks and sources. An analogous picture was obtained in the case of *diffusion screening theory* of Ostwald ripening [21–26], where similar screened diffusion-mediated interactions were derived from a coarse-graining of second-phase particles. In this context, screened diffusive interactions were originally employed as a tool to avoid divergences for finite volume fractions of particles due to the infinite-range Laplacian field.

In our case, the coarse grained diffusion field that generates screened interactions allows us to effectively account for the limited information about the distributions of small defect clusters.

In a dilute configuration of cavities, each of them can be approximated as a point source with an effective sink strength given by $Q_i = 4\pi R_i^2\dot{R}_i$. A formal solution of Eq. (38) is then

$$\bar{c}(\mathbf{x}) = \sum_{i=1}^N Q_i G_Y(|\mathbf{x}-\mathbf{x}_i|;\overline{\xi_\Delta}) - \overline{\xi_\Delta c_\Delta} \times \int dV' G_Y(|\mathbf{x}-\mathbf{x}_i|;\overline{\xi_\Delta}) + c_\infty, \tag{41}$$

where $\mathbf{x}_i$ denotes the center of the ith cavity. We note that

$$-\overline{\xi_\Delta c_\Delta}\int dV' G_Y(|\mathbf{x}-\mathbf{x}'|;\overline{\xi_\Delta}) = \frac{\overline{\xi_\Delta c_\Delta}}{\overline{\xi_\Delta}} = \frac{\int_b^\infty dR\,\xi_\Delta(R)f(R)c_\Delta(R)}{\int_b^\infty dR\,\xi_\Delta(R)f(R)} = \langle c_\Delta\rangle, \tag{42}$$

where the average $\langle\ldots\rangle$ is defined with respect to the weighted distribution $\tilde{f}(R) = \xi_\Delta(R)f(R)$.

Thus, we arrive at the following self-consistent relation between the rates of change of the cavity radii $\dot{R}_i$, the vacancy field, and the distribution of the interstitial dislocation loops $f(R)$:

$$\bar{c}(\mathbf{x}) = -\sum_{i=1}^N R_i^2\dot{R}_i \frac{\exp[-\sqrt{\overline{\xi_\Delta}/D_v}|\mathbf{x}-\mathbf{x}_i|]}{D_v|\mathbf{x}-\mathbf{x}_i|} + c_\infty + \langle c_\Delta\rangle. \tag{43}$$

To solve this equation the vacancy concentration has to be evaluated at the position of each cavity, satisfying the boundary condition of local thermodynamic equilibrium, i.e.,

$$c_\Sigma(R_i) = -\sum_{\substack{j=1\\ j\neq i}}^N R_j^2\dot{R}_j \frac{\exp[-\sqrt{\overline{\xi_\Delta}/D_v}|\mathbf{x}_i-\mathbf{x}_j|]}{D_v|\mathbf{x}_i-\mathbf{x}_j|} - \frac{R_i\dot{R}_i}{D_v} + c_\infty + \langle c_\Delta\rangle, \qquad i = 1,\ldots,N, \tag{44}$$

where $-\frac{R_i\dot{R}_i}{D_v}$ is a finite size correction accounting for the self-diffusional interaction of a cavity with itself, representing vacancies propagating between different points on the surface of the same cavity. As a comparison, we recall the analogous of the above system of equations for a system where the n dislocation loops are explicitly considered as discrete objects, given by the set of $N+n$ equations [15]:

$$c_\Sigma(R_i) = -\sum_{\substack{j=1\\ j\neq i}}^N \frac{R_j^2\dot{R}_j}{D_v|\mathbf{x}_i-\mathbf{x}_j|} - \frac{R_i\dot{R}_i}{D_v} + \sum_{k=N+1}^{N+n}\frac{b_e R_k\dot{R}_k}{2D_v|\mathbf{x}_i-\mathbf{x}_k|} + c_\infty, \qquad i = 1,\ldots,N$$
$$c_\Delta(R_i) = -\sum_{j=1}^N \frac{R_j^2\dot{R}_j}{D_v|\mathbf{x}_i-\mathbf{x}_j|} + \sum_{\substack{k=N+1\\ k\neq i}}^{N+n}\frac{b_e R_k\dot{R}_k}{2D_v|\mathbf{x}_i-\mathbf{x}_k|} - \frac{b_e\ln\left(\frac{8R_i}{r_d}\right)\dot{R}_i}{2\pi D_v} + c_\infty, \qquad i = N+1,\ldots,N+n, \tag{45}$$

where the indices from 1 to N denote cavities and from $N+1$ to $N+n$ denote dislocation loops. By inverting the linear system defined by Eq. (44), the set of $\dot{R}_i$ can be then calculated provided $f(R)$ is known.

The screening length changes with time because it depends on the evolution of the distribution of the interstitial loop sizes. Let the time-dependent size distribution function be $F(R,t)$. A continuity equation in particle-size space for the distribution $F(R,t)$ can be written as

$$\frac{\partial F(R,t)}{\partial t} + \frac{\partial [F(R,t) v_{\rm il}(R,t)]}{\partial R} = \dot{n}(R,t), \tag{46}$$

where $\dot{n}(R,t)$ is the net rate at which loops of radius R are created, as a result of coalescence of existing loops and nucleation of new loops. The growth rate $v_{\rm il}(R,t)$ of a loop of radius R at time t is given by

$$v_{\rm il}(R,t) = -[c_{\rm avg}(t) - c_\Delta(R)] \frac{2\pi D_v}{b_e \ln(8R/r_d)}, \tag{47}$$

where $c_{\rm avg}(t)$ is the spatially averaged vacancy concentration. Differentiating with respect to R gives

$$\frac{\partial v_{\rm il}(R,t)}{\partial R} = \frac{2\pi D_v}{b_e \ln(8R/r_d)} \left\{ \frac{[c_{\rm avg}(t) - c_\Delta(R)]}{R \ln(8R/r_d)} + \frac{\mu b_e \Omega c_\Delta(R)}{4\pi(1-\nu) R^2 k_B T} \left[\ln\left(\frac{8R}{r_d}\right) - 2 \right] \right\}. \tag{48}$$

In the homogeneous mean field treatment, the term $c_{\rm avg}(t)$ can be obtained by averaging Eq. (43) with respect to $\mathbf{x}$:

$$\begin{aligned} c_{\rm avg}(t) &= -\lim_{V\to\infty} \left\{ \sum_{i=1}^{N} \frac{R_i^2(t)\dot{R}_i(t)}{V D_v} \int_V d^3x \frac{\exp[-\sqrt{\overline{\xi_\Delta}/D_v}|\mathbf{x}-\mathbf{x}_i|]}{|\mathbf{x}-\mathbf{x}_i|} \right\} + c_\infty + \langle c_\Delta \rangle \\ &= \langle c_\Delta \rangle + c_\infty - \frac{4\pi\rho_c}{\overline{\xi_\Delta}} \left(\frac{1}{N} \sum_{i=1}^{N} R_i^2(t)\dot{R}_i(t) \right) = \langle c_\Delta \rangle + c_\infty - \frac{\overline{\dot{V}}_c(t)\rho_c}{\overline{\xi_\Delta}}, \end{aligned} \tag{49}$$

where ρ_c denotes the number density of cavities and $\overline{\dot{V}}_c(t)$ denotes the average rate of change of the volume of cavities, at time t. It is clear that in the limiting case of $\overline{\xi_\Delta} = 0$ the above expression diverges, and the integral of the Green's function has to be performed up to a suitable cutoff distance.

In summary, while the mean field of interstitial loops screens the diffusive interaction between cavities, the rate of growth of cavities also determines the evolution of the mean field: the cavities and the mean field are coupled. In Fig. 5 we show a flowchart that summarizes a scheme to compute the system evolution, highlighting the couplings between the cavities and the mean field.

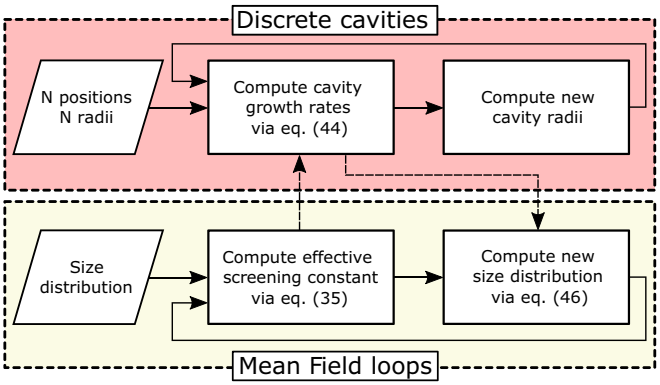

FIG. 5. Flowchart summarizing a scheme to compute the evolution of the coupled mean field of interstitial loops and discrete cavities.

D. Numerical estimate of the screening length

In this section we calculate the initial value, at $t = 0$, of the screening length of the effective interaction between cavities in the presence of a mean field of interstitial dislocation loops. It is helpful to introduce the scaled distribution function:

$$A\phi\left(\frac{R}{b}, t\right) = F(R,t), \tag{50}$$

where A is a normalization factor with the dimensions of length^{-4}, defined with respect to the size distribution at $t = 0$ as

$$A = \rho(0) \left(b \int_1^\infty du\, \phi(u,0) \right)^{-1}, \tag{51}$$

where $\rho(t)$ is the number density of the mean field clusters at time t. The screening length $\Delta l = \sqrt{D_v/\overline{\xi_\Delta}}$, at time $t = 0$, is given by

$$\begin{aligned} \Delta l(0) &= \left(\int_b^\infty dR\, \xi_\Delta(R) F(R,t)/D_v \right)^{-1/2} \\ &= \frac{1}{2\pi b\sqrt{A}} \left(\int_1^\infty du\, u\, \phi(u,0)/\ln(8bu/r_d) \right)^{-1/2} \end{aligned} \tag{52}$$

For the initial loop size distribution we assume a power law with an exponentially decaying cutoff at small loop radii, i.e.,

$$\phi(u,0) = e^{-c_1/u} u^{-c_2}, \tag{53}$$

where c_1 and c_2 are constants. To ensure the existence of the integrals defining $\overline{\xi_\Delta}$ and $\overline{\xi_\Delta c}$ we require $c_2 > 2$.

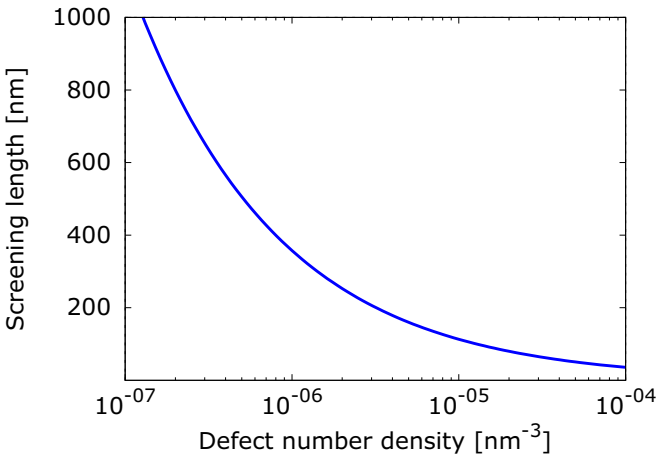

FIG. 6. Plot of the prefactor $(2\pi)^{-1}(\rho(0)b)^{-1/2}$ of Eq. (54) as a function of loop number density ρ. The value of the Burgers vector b is 0.27 nm, which is representative of tungsten.

The screening length can then be recast as

$$\Delta l(0) \approx \frac{1}{2\pi\sqrt{\rho(0)b}}\sqrt{\frac{\int_1^\infty du\ \exp(-c_1/u)u^{-c_2}}{\int_1^\infty du\ \exp(-c_1/u)u^{-c_2+1}/\ln(8ub/r_d)}} \equiv \frac{\Pi(c_1,c_2)}{2\pi\sqrt{\rho(0)b}}, \tag{54}$$

where we have separated the dependence on the loop number density from the shape of the size distribution contained in $\Pi(c_1, c_2)$. For realistic loop densities of 10^{-6}–10^{-4} nm^{-3} the factor $(2\pi\sqrt{\rho(0)b})^{-1}$ is of the order of 10^2–10^3 nm (see Fig. 6), while $\Pi(c_1, c_2)$ is of the order of unity for reasonable values of c_1 and c_2. In particular, with $0.1 < c1 < 1$ and $2 < c2 < 4$, we have $0.68 \lesssim \Pi \lesssim 1.3$. At these loop densities the screening length is comparable to the separation of the loops, which may be substantially smaller than the separation of cavities. Therefore the screening of the diffusive interaction between cavities by small dislocation loops plays a significant role in the evolution of the distribution of cavity sizes during an anneal.

IV. EXTENSION TO THIN FILM GEOMETRY

Transmission electron microscopy is providing accurate data on the distributions of radiation defects [2,47]. Since TEM samples are always thin films we provide in this section an extension of the theory to infinitely extended thin films.

Consider a region $V \in \mathbb{R}^3$ infinitely extended in the $\hat{x}$ and $\hat{y}$ directions and of thickness H in the $\hat{z}$ direction, i.e., $V = \{(x, y, z) \in \mathbb{R}^3 : x \in \mathbb{R}, y \in \mathbb{R}, -H/2 < z < H/2\}$. We define a $L \times L \times H$ cell $\Gamma(0) = \{\mathbf{x} = x_1\mathbf{a}_1 + x_2\mathbf{a}_2 + x_3\mathbf{a}_3 : -1/2 < x_\alpha < 1/2, \alpha = 1, 2, 3\}$, where $\mathbf{a}_1 = (L, 0, 0)$, $\mathbf{a}_2 = (0, L, 0)$, and $\mathbf{a}_3 = (0, 0, H)$ are the three basis vectors defining the cell. The cell $\Gamma(0)$ contains N spherical cavities and a much larger number of smaller circular prismatic dislocation loops, with size distribution function $f(R)$, normalized to the loop number density. The primitive cell is infinitely replicated in the $\hat{x}$ and $\hat{y}$ directions.

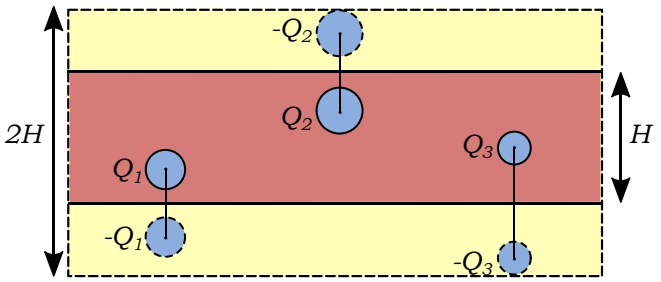

FIG. 7. 2D sketch of the primitive cell structure for the thin film configuration. The red shaded region is a repeat cell of the thin film. Image clusters (portrayed with dashed boundaries) of opposite effective charge are constructed in the yellow shaded regions and the original primitive cell is extended accordingly. Periodic boundary conditions are imposed on the dashed boundaries and in the directions perpendicular to the drawing. The size of cavities with respect to the simulation cell is exaggerated for clarity.

Let Σ_i denote the surface of the ith cavity. We impose the following boundary conditions on the vacancy concentration field $c(\mathbf{x})$:

$$\begin{aligned} c(x, y, -H/2) = c(x, y, H/2) = c_S, \\ c(\mathbf{x} \in \Sigma_i) = c_{\Sigma_i} \qquad i = 1, \ldots, N. \end{aligned} \tag{55}$$

Using the terminology of electrostatics, each cavity can be associated with an effective charge Q, related to rate of growth of the cavity volume $\mathcal{V}$:

$$Q_i = -\frac{d\mathcal{V}_i}{dt} = 4\pi R_i^2 \frac{dR_i}{dt}, \tag{56}$$

where R_i is the radius of the ith cavity. As noted in the previous section, to first order the effect of the mean field of dislocation loops is to introduce a screened interaction with screening length $\sqrt{D_v/\overline{\xi_\Delta}(t)}$, and to displace the resultant concentration field by an amount

$$\langle c_\Delta \rangle(t) = \frac{\int dR \xi_\Delta(R) F(R,t) c_\Delta(R)}{\int dR \xi_\Delta(R) F(R,t)}.$$

The boundary conditions at $c(z = \pm H/2) = c_S$ can be satisfied using the method of images, by introducing an infinite number of periodic images of the thin film in the $\hat{z}$ directions. The images are constructed as follows: we extend the primitive cell by $H/2$ in the positive and negative $\hat{z}$ directions; for each cavity with charge Q in the original primitive cell located at (x, y, z) we add a virtual cavity of charge $-Q$ at $(x, y, \mathrm{sgn}(z)H - z)$. A new primitive cell may then be defined containing $2N$ interacting cavities: $\Gamma(0) = \{\mathbf{x} = x_1\mathbf{a}_1 + x_2\mathbf{a}_2 + x_3\mathbf{a}_3 : -1/2 < x_\alpha < 1/2, \alpha = 1, 2, 3\}$, with primitive vectors $\mathbf{a}_1 = (L, 0, 0)$, $\mathbf{a}_2 = (0, L, 0)$, and $\mathbf{a}_3 = (0, 0, 2H)$. A two-dimensional (2D) sketch of such a construction is presented in Fig. 7. This new primitive cell is charge neutral by construction, and it is repeated infinitely many times along z.

The self-consistent system of equations that determines the set of $\{Q_i\}_{i=1,\ldots,N}$ at time t is therefore given by

$$\begin{aligned} c_{\Sigma_i} = &\sum_{\substack{j=1\\ j\neq i}}^{N} Q_j \Bigg[{\sum_{\mathbf{m}}}' G_Y(|\mathbf{x}_i - \mathbf{m} + \mathbf{x}_j|; \overline{\xi_\Delta}) \\ &- \sum_{\mathbf{m}} G_Y(|\mathbf{x}_i - \mathbf{m} + \bar{\mathbf{x}}_j|; \overline{\xi_\Delta}) \Bigg] \\ &- \frac{Q_i}{4\pi D_v R_i} + c_S + \langle c_\Delta \rangle, \\ i = 1, \ldots, N, \end{aligned} \tag{57}$$

where $\mathbf{m} = m_1\mathbf{a}_1 + m_2\mathbf{a}_2 + m_3\mathbf{a}_3$, $m_\alpha \in \mathbb{Z}$, $\alpha = 1, 2, 3$, $\bar{\mathbf{x}}_j = (x_j, y_j, \mathrm{sgn}(z_j)H - z_j)$ and primed sums denote that the term $\mathbf{m} = \mathbf{0}$ is not included when $\mathbf{x}_i = \mathbf{x}_j$.

The sums over $\mathbf{m}$ are convergent for finite values of the screening length. However, it is possible that the mean field loops disappear during an anneal, leading to an infinite screening length and therefore to a $1/r$ diffusive interaction between the cavities. In that case, the sums over $\mathbf{m}$ are only *conditionally* convergent.

Since the new primitive cell is charge neutral, we may use a variant of the Ewald summation technique to derive an absolutely convergent series for all screening lengths. This can be achieved by introducing the following kernel:

$$\begin{aligned} K(\mathbf{x}_i, \mathbf{x}_j; \epsilon) = &- \sum_{\mathbf{k}} \frac{\exp[-(k^2+\epsilon^2)/4\beta^2]}{V D_v (k^2+\epsilon^2)} e^{i\mathbf{k}\cdot\mathbf{x}_i} [e^{-i\mathbf{k}\cdot\mathbf{x}_j} - e^{-i\mathbf{k}\cdot\bar{\mathbf{x}}_j}] \\ &- \frac{1}{8\pi D_v} \Bigg\{ {\sum_{\mathbf{m}}}' \frac{1}{|\mathbf{x}_i - \mathbf{x}_j + \mathbf{m}|} \Bigg[\mathrm{erfc}\left(\beta|\mathbf{x}_i - \mathbf{x}_j + \mathbf{m}| + \frac{\epsilon}{2\beta}\right) e^{\epsilon|\mathbf{x}_i - \mathbf{x}_j + \mathbf{m}|} \\ &+ \mathrm{erfc}\left(\beta|\mathbf{x}_i - \mathbf{x}_j + \mathbf{m}| - \frac{\epsilon}{2\beta}\right) e^{-\epsilon|\mathbf{x}_i - \mathbf{x}_j + \mathbf{m}|} \Bigg] \\ &- \sum_{\mathbf{m}} \frac{1}{|\mathbf{x}_i - \bar{\mathbf{x}}_j + \mathbf{m}|} \Bigg[\mathrm{erfc}\left(\beta|\mathbf{x}_i - \bar{\mathbf{x}}_j + \mathbf{m}| + \frac{\epsilon}{2\beta}\right) e^{\epsilon|\mathbf{x}_i - \bar{\mathbf{x}}_j + \mathbf{m}|} \\ &+ \mathrm{erfc}\left(\beta|\mathbf{x}_i - \bar{\mathbf{x}}_j + \mathbf{m}| - \frac{\epsilon}{2\beta}\right) e^{-\epsilon|\mathbf{x}_i - \bar{\mathbf{x}}_j + \mathbf{m}|} \Bigg] \Bigg\} + \frac{\delta_{ij}}{4\pi D_v} \left[\frac{2\beta e^{-\epsilon^2/4\beta^2}}{\sqrt{\pi}} - \epsilon\, \mathrm{erfc}\left(\frac{\epsilon}{2\beta}\right) \right]. \end{aligned} \tag{58}$$

The set of self-consistent equations to be solved become

$$c_{\Sigma_i} = \sum_{\substack{j=1\\ j\neq i}}^{N} Q_j K(\mathbf{x}_i, \mathbf{x}_j; \sqrt{\overline{\xi_\Delta}/D_v}) - \frac{Q_i}{4\pi D_v R_i} + c_S + \langle c_\Delta \rangle, \qquad i = 1, \ldots, N, \tag{59}$$

which is the analog of Eq. (44) for the thin film configuration. A detailed derivation of $K(\mathbf{x}_i, \mathbf{x}_j; \epsilon)$ is given in Appendix C.

We note that the numerical scheme to compute the temporal evolution of cavities remains the same as that presented at the end of Sec. III.

By taking the limit in the kernel of an infinite screening length we obtain

$$\begin{aligned} \lim_{\epsilon\to 0} K(\mathbf{x}_i, \mathbf{x}_j, \epsilon) = &- \sum_{\mathbf{k}} \frac{\exp[-k^2/4\beta^2]}{V D_v k^2} e^{i\mathbf{k}\cdot\mathbf{x}_i} [e^{-i\mathbf{k}\cdot\mathbf{x}_j} - e^{-i\mathbf{k}\cdot\bar{\mathbf{x}}_j}] \\ &- \frac{1}{4\pi D_v} \left[{\sum_{\mathbf{m}}}' \frac{\mathrm{erfc}(\beta|\mathbf{x}_i - \mathbf{x}_j + \mathbf{m}|)}{|\mathbf{x}_i - \mathbf{x}_j + \mathbf{m}|} - \sum_{\mathbf{m}} \frac{\mathrm{erfc}(\beta|\mathbf{x}_i - \bar{\mathbf{x}}_j + \mathbf{m}|)}{|\mathbf{x}_i - \bar{\mathbf{x}}_j + \mathbf{m}|} \right] + \delta_{ij} \frac{2\beta}{4\pi^{3/2} D_v}, \end{aligned} \tag{60}$$

which is the usual expression for the Ewald sum for the unscreened Green's function $G(|\mathbf{x} - \mathbf{x}'|) = -(4\pi D_v|\mathbf{x} - \mathbf{x}'|)^{-1}$. Thus the kernel $K(\mathbf{x}_i, \mathbf{x}_j; \epsilon)$ enables us to treat within the same set of equations the evolution of cavities, whatever the screening length.

V. FULL MEAN FIELD DESCRIPTION

In this section we consider both dislocation loops and cavities as contributors to a mean field. This may be useful whenever information on cluster distributions at all length scales is incomplete. Consider the vacancy field generated by a spherical cavity in an infinite homogeneous medium in which the vacancy concentration far from the cavity is c_∞:

$$\begin{aligned} c(r) &= c_\infty - [c_\infty - c_\Sigma(R)]\frac{R}{r} \\ &= c_\infty + \xi_\Sigma(R) G(r) [c_\infty - c_\Sigma(R)], \end{aligned} \tag{61}$$

where $\xi_\Sigma(R) = 4\pi D_v R$ and

$$c_\Sigma(R) = c_0 \exp\left[\frac{2\gamma\Omega}{R k_B T}\right]. \tag{62}$$

Consider the case of a spatially homogeneous, uncorrelated distribution of loops and cavities. We define the number density respectively of vacancy loops, interstitial loops, and cavities, with radii in the range $(R + dR)$, as $f_{\rm v}(R)dR$, $f_{\rm i}(R)dR$, and $f_c(R)dR$.

Following a similar treatment to that used in Sec. III, we can write a mean field equation analogous to that of Eq. (34):

$$\begin{aligned}\bar{c}(\mathbf{x}) = c_\infty + \int dV' G(|\mathbf{x}-\mathbf{x}'|) \int_b^\infty dR\, \{&\xi_\Delta(R) f_{\rm v}(R) \\ &\times [\bar{c}(\mathbf{x}') - c_\Delta^{\rm v}(R)] + \xi_\Delta(R) f_{\rm i}(R)[\bar{c}(\mathbf{x}') - c_\Delta^{\rm i}(R)] \\ &+ \xi_\Sigma(R) f_c(R)[\bar{c}(\mathbf{x}') - c_\Sigma(R)]\},\end{aligned} \tag{63}$$

where the boundary condition $c_\Delta^{\rm v}(R)$ for vacancy loops differs from that for interstitial loops, $c_\Delta^{\rm i}(R)$, by the sign in the exponent, i.e., $c_\Delta^{\rm v}(R) c_\Delta^{\rm i}(R) = c_0^2$.

We define the quantities $c_1 = c_\Delta^v$, $c_2 = c_\Delta^i$, $c_3 = c_\Sigma$, $f_1 = f_v$, $f_2 = f_i$, $f_3 = f_c$, $\xi_1 = \xi_2 = \xi_\Delta$, and $\xi_3 = \xi_\Sigma$. Equation (63) then assumes the compact form:

$$\begin{aligned}\bar{c}(\mathbf{x}) = c_\infty + \sum_{\alpha=1}^{3} \int dV' G(|\mathbf{x}-\mathbf{x}'|) \\ \times \int_b^\infty dR\, \xi_\alpha(R) f_\alpha(R)[\bar{c}(\mathbf{x}') - c_\alpha(R)].\end{aligned} \tag{64}$$

We define

$$\begin{aligned}\overline{\xi} &= \sum_{\alpha=1}^{3} \overline{\xi_\alpha} = \sum_{\alpha=1}^{3} \int_b^\infty dR\, \xi_\alpha(R) f_\alpha(R), \\ \overline{\xi c} &= \sum_{\alpha=1}^{3} \overline{\xi_\alpha c_\alpha} = \sum_{\alpha=1}^{3} \int_b^\infty dR \xi_\alpha(R) f_\alpha(R) c_\alpha(R),\end{aligned} \tag{65}$$

so that

$$\begin{aligned}\bar{c}(\mathbf{x}) = c_\infty + \overline{\xi} \int dV' G(|\mathbf{x}-\mathbf{x}'|)\bar{c}(\mathbf{x}') \\ - \overline{\xi c} \int dV' G(|\mathbf{x}-\mathbf{x}'|).\end{aligned} \tag{66}$$

In momentum space, using the Fourier transform definition $f(\mathbf{x}) = (2\pi)^{-3/2} \int d\mathbf{q} e^{i\mathbf{q}\cdot\mathbf{x}} \tilde{f}(\mathbf{q})$, this becomes

$$\tilde{\bar{c}}(\mathbf{q}) = \tilde{c}_\infty + \overline{\xi} \tilde{G}(\mathbf{q}) \tilde{\bar{c}}(\mathbf{q}) - (2\pi)^{3/2} \overline{\xi c} \tilde{G}(\mathbf{q}) \delta(\mathbf{q}), \tag{67}$$

leading to the solution

$$\tilde{\bar{c}}(\mathbf{q}) = \frac{\tilde{c}_\infty - (2\pi)^{3/2} \overline{\xi c} \tilde{G}(\mathbf{q}) \delta(\mathbf{q})}{1 - \overline{\xi} \tilde{G}(\mathbf{q})}. \tag{68}$$

In a homogeneous infinite medium, we have $G(|\mathbf{x}-\mathbf{x}'|) = -1/(4\pi D_v |\mathbf{x}-\mathbf{x}'|)$ leading to

$$\begin{aligned}\tilde{\bar{c}}(\mathbf{q}) &= \delta(\mathbf{q}) \frac{D_v c_\infty + (2\pi)^{3/2} \overline{\xi c}/q^2}{D_v + \overline{\xi}/q^2} \\ &= \frac{\delta(q)}{2\pi} \frac{D_v c_\infty + (2\pi)^{3/2} \overline{\xi c}/q^2}{D_v q^2 + \overline{\xi}},\end{aligned} \tag{69}$$

and, transforming back in real space,

$$\begin{aligned}\int \frac{d\mathbf{q}}{(2\pi)^{3/2}} e^{i\mathbf{q}\cdot\mathbf{x}} \tilde{\bar{c}}(\mathbf{q}) \\ = \frac{1}{(2\pi)^{5/2}} \int_0^\infty dq \int_0^\pi \sin\phi\, d\phi \int_{-\pi}^{\pi} d\theta \delta(q) \\ \times \frac{D_v q^2 c_\infty + (2\pi)^{3/2} \overline{\xi c}}{D_v q^2 + \overline{\xi}} e^{iqr\cos\phi} = \frac{\overline{\xi c}}{\overline{\xi}},\end{aligned} \tag{70}$$

which implicitly depends on time through the size distribution functions $f_\alpha(R)$. We point out that for $f_\alpha(R) = \delta_{\alpha 2} f(R)$ we recover the result of the previous sections.

The evolution laws for the size distributions are analogous to Eq. (46), where the growth velocities are given by

$$\begin{aligned}v_{\rm vl}(R,t) &= \left[\bar{c}(t) - c_\Delta^{\rm v}(R)\right] \frac{2\pi D_v}{b \ln\left(\frac{8R}{r_d}\right)}, \\ v_{\rm il}(R,t) &= -\left[\bar{c}(t) - c_\Delta^{\rm i}(R)\right] \frac{2\pi D_v}{b \ln\left(\frac{8R}{r_d}\right)}, \\ v_{\rm c}(R,t) &= -[\bar{c}(t) - c_\Sigma(R)] \frac{D_v}{R},\end{aligned} \tag{71}$$

respectively for vacancy loops, interstitial loops, and cavities.

As a consequence, the average vacancy concentration depends on time through the time-dependent size distribution functions $F_\alpha(R,t)$ as

$$\bar{c}(t) = \frac{\overline{\xi c}(t)}{\overline{\xi}(t)} = \frac{\sum_{\alpha=1}^{3} \int_b^\infty dR\, \xi_\alpha(R) F_\alpha(R,t)}{\sum_{\alpha=1}^{3} \int_b^\infty dR\, \xi_\alpha(R) F_\alpha(R,t) c_\alpha(R)}. \tag{72}$$

A numerical scheme for the computation of the cluster size distribution as a function of time can then be summarized as follows:

(1) Starting from the size distributions $f_{\rm v}(R,t_0)$, $f_{\rm i}(R,t_0)$, and $g(R,t_0)$, compute $c(t_0)$ via Eq. (70).

(2) Compute the new size distributions at time $t_0 + dt$ using Eq. (46).

(3) Reiterate from step (1).

VI. NUMERICAL SIMULATIONS

We present simulations of an anneal of an infinite thin film of thickness $H = 200$ nm with 30 cavities per periodic cell, using the technique presented in Sec. IV, for tungsten, iron, and beryllium. The sizes L of the primitive cell in both the x and y directions are respectively 133.64, 422.58, and 2112.89 for the simulations with cavity densities of 10^{-5} nm^{-3}, 10^{-6} nm^{-3} and 4×10^{-8} nm^{-3}.

We compared the effect of three mean field conditions: containing only interstitial loops, or only vacancy loops, or no loops. The initial size distribution of the loops was $\phi(R) = (b/R)^{c_2} \exp(-c_1 b/R)$, $c_1 = 0.2$, $c_2 = 3$ and normalization such that the loop number density at $t = 0$ was 10^{-4} nm^{-3}, therefore the average separation between loops was ~ 22 nm.

The cavities were assigned to random positions in the periodic cell, satisfying the number density and a minimum separation between cavities of 10 nm, with sizes taken from a Gaussian distribution of mean 1 nm and standard deviation 0.1 nm. No vacancy supersaturation was assumed in the film, so that its free surfaces were assigned a constant vacancy concentration equal to the equilibrium value c_0.

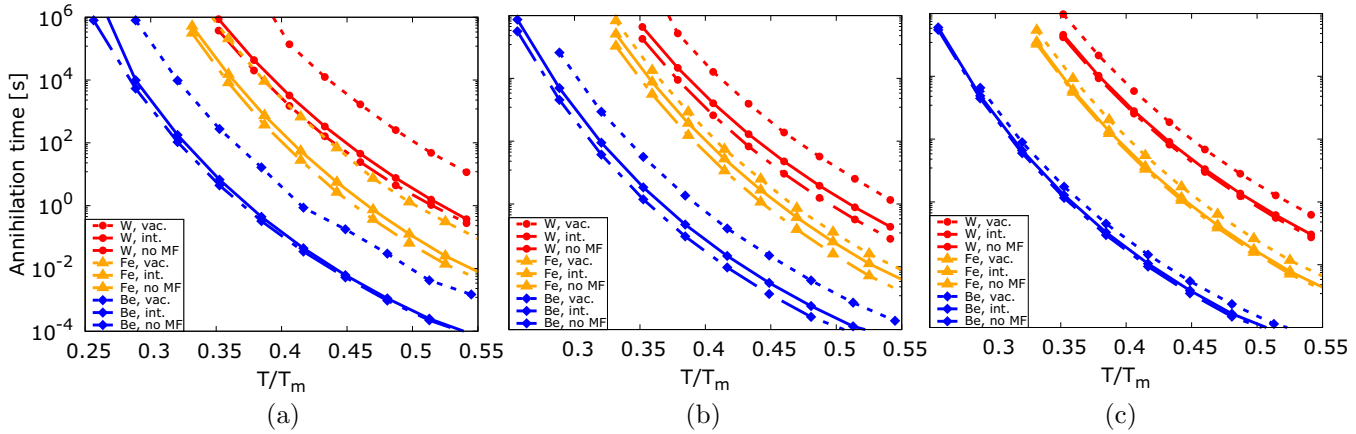

FIG. 8. Time taken to remove all cavities in thin films of thickness 200 nm in tungsten (red, circles), bcc iron (orange, triangles), and beryllium (blue, diamonds), as a function of annealing homologous temperature, for three number densities of cavities: (a) 10^{-5} nm^{-3}, (b) 10^{-6} nm^{-3}, and (c) 4×10^{-8} nm^{-3}. In each case there are either no dislocation loops present (solid lines), or only vacancy loops (dashed lines) or only interstitial loops (dotted solid-dashed lines). Diffusion is assumed to occur by a vacancy mechanism only.

In Fig. 8 we plot the time taken to remove all the cavities, as a function of homologous annealing temperature T/T_{m}.

We see that the time-scale estimates given in Sec. II are in broad agreement with numerical simulations, for all three investigated materials. As already noted in our previous work [15], we see that as the number density of cavities increases the time to annihilate all cavities also increases. This is due to the diffusive interaction between cavities: as the distances between cavities are reduced, the local vacancy concentration between cavities increases. The driving force for vacancy emission from each cavity is then reduced compared to the case of a dilute configuration of cavities.

The presence of a mean field of dislocation loops, as previously discussed, introduces a screening of the diffusive interaction between cavities *and* increases of the overall background vacancy concentration. Screening accelerates the annihilation of cavities, while the increased vacancy concentration has the opposite effect, and can even induce a transient phase of cavity growth. Whether one effect or the other dominates depends on the type of dislocation loops that make up the mean field.

We have assumed that the only mobile point defects are vacancies. The concentrations of these point defects just outside interstitial and vacancy loops are highly asymmetrical due to the exponential dependence on the climb force and the change of sign of the Burgers vector between the loops. As a consequence, the vacancy concentration near interstitial loops is much less than for vacancy loops. Therefore the rate of evolution of vacancy loops is faster than that of interstitial loops.

The screening factor and the larger background vacancy concentration provided by vacancy loops suggest that they might affect the evolution of cavities to a higher degree than interstitial loops. However, it should also be kept in mind that the evolution by vacancy diffusion of vacancy loops is faster than that of interstitial loops with the same initial distributions of loop sizes, and by the end of the simulation a large fraction of the initial vacancy loop population has evaporated. To illustrate this behavior, we plot in Fig. 9 the time required for the vacancy loops screening coefficient $\sqrt{\xi/D_v}$ to halve with respect to its initial value, as a function of simulated temperature. We point out that the "half-lives" of the screening coefficient are always much shorter than the time required for all cavities to evaporate. The evolution of the vacancy loops mean field does not appear to be noticeably affected by the number density of cavities, at least in the investigated density range from 4×10^{-8} to 10^{-5} nm^{-3}.

In simulations with only interstitial loops as part of the mean field, on the other hand, the initial size distribution function, the screening coefficient, and the shift to the background vacancy concentration are practically constant with respect to the evolution of cavities.

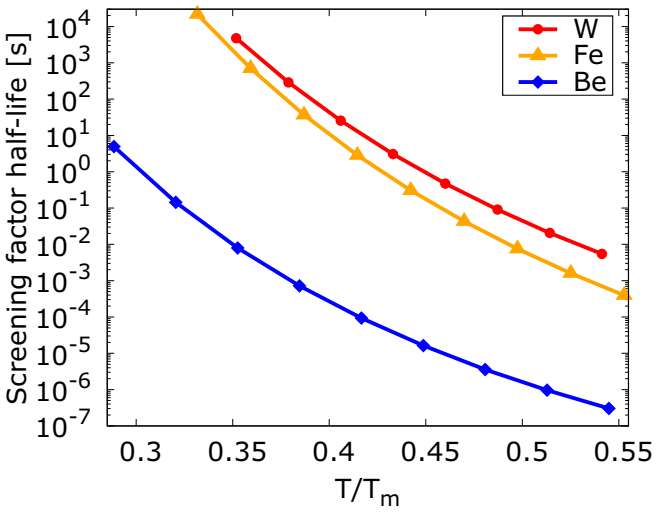

FIG. 9. Time taken to halve the screening factor $\sqrt{\xi/D_v}$ with respect to its initial value, in thin films of thickness 200 nm in tungsten (red, circles), bcc iron (orange, triangles), and beryllium (blue, diamonds), with a mean field of vacancy loops, as a function of annealing homologous temperature. The initial cavity and dislocation loop number densities are respectively 10^{-5} nm^{-3} and 10^{-4} nm^{-3}.

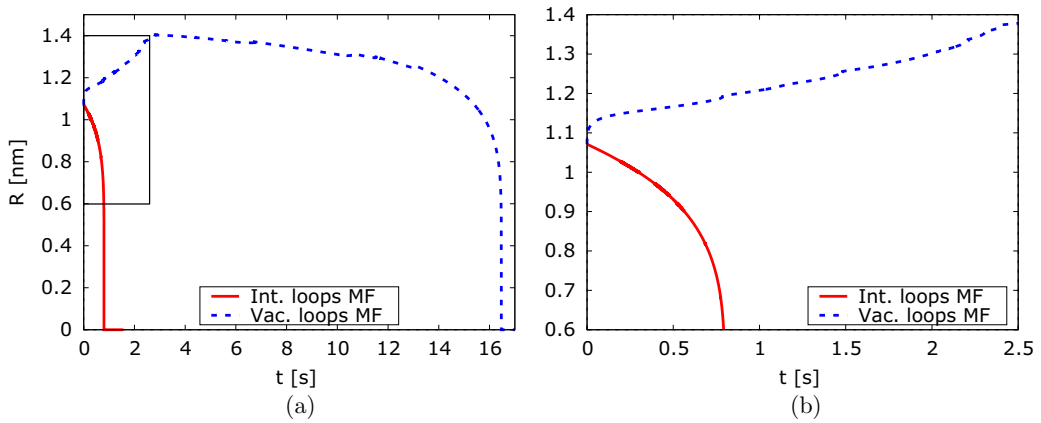

FIG. 10. Evolution of the radius of a single cavity at $z = 0.39H$ as a function of time for tungsten at 1800 K and for a cavity number density of 10^{-6} nm^{-3}. Results are compared for the case of an interstitial loop mean field (solid red lines), and a vacancy loop mean field (dashed blue lines). Plot (b) is a magnification of the boxed area of plot (a).

According to our simulations, when the mean field is made of interstitial loops there is a systematic decrease of cavity evaporation time scales with respect to the reference values, for every investigated cavity number density. We must conclude that the screening effect, partially suppressing the diffusive interaction between cavities, is the dominant one for interstitial loops. The opposite holds true for the vacancy loops mean field simulations, where a systematic and very pronounced *increase* in cavity evaporation time scales suggests that the extra background vacancy concentration plays the most important role.

In order to further elucidate this point, we show in Fig. 10 the evolution in time of the size of a single cavity in tungsten at 1800 K and with a cavity number density of 10^{-6} nm^{-3}. The cavity is located at $z = 0.39H$. We note that in the initial phases of the simulation the additional background vacancy concentration induced by vacancy loops results in the cavity rapidly *adsorbing* vacancies. As the mean field evolves, vacancy loops decrease in number and the extra vacancy concentration is reduced until the surface energy of cavities becomes the dominant driving force, leading to their evaporation. Due to the initial phase of growth of the cavity, the total annihilation time with the vacancy loops mean field is therefore larger than in the case of the interstitial loops mean field. While we found this to hold true for all investigated cavity densities, the picture is slightly more complex when only considering the evolution of a single cavity of the ensemble. In particular, the *same* cavity will not always evaporate faster with an interstitial loop mean field, especially in simulations with a high cavity density.

To illustrate such a case, we present in Fig. 11 the evolution of a single cavity at $z = 0.65H$, with a cavity number density 10^{-5} nm^{-3} and at a temperature of 1800 K. As we can see, the vacancy loops mean field still induces an initial phase of cavity growth (Fig. 11), but the cavity evolves erratically in the interstitial loops mean field simulation. By comparing Fig. 11(b) with a real-space view of the simulation (Fig. 12) we find this behavior is most likely due to local interaction between cavities.

In particular, the erratic size increases and decreases of the cavity seem to be correlated with the evaporation of cavities in its neighborhood. Such local effects are much less important with the vacancy loops mean field because, even though the shift in background vacancy concentration dominates, the screening coefficient is still substantially larger than for interstitial loops, as already mentioned. This suggests that at higher densities local interactions between cavities play a large role and might lead the dynamics of single cavities to deviate from the general behavior with respect to mean field conditions.

VII. CONCLUSIONS

In this paper we derived a hybrid mean field and real-space model that couples our earlier [15] nonlocal model of evolution of cavities produced by irradiation with a mean field representing dislocation loops smaller than the experimental detection limit. The main result is that the mean field screens the diffusive interactions between cavities and adds to, or subtracts from, the vacancy concentration depending on whether the loops are vacancy or interstitial character respectively. We presented a general scheme to implement higher order corrections to the model. The model was initially derived for an infinite medium, but it was then modified to treat the case of an infinitely extended thin film, which is more useful for comparing with available experimental data obtained by transmission electron microscopy. Through preliminary numerical simulations we discussed some of the features of the model, highlighting in particular the interplay between the evolution of the mean field and the cavities, and the roles of the cavity number density and mean fields comprising vacancy vs interstitial loops.

Finally, we mention some avenues for development of the model. In its current state, we have assumed cavities and dislocation loops are immobile, with only their sizes as dynamical variables. However, nanometric dislocation loops in bcc metals have been experimentally observed [48] to perform fast, one-dimensional diffusion. Theoretical investigations [49] have also shown that interstitial loops in bcc

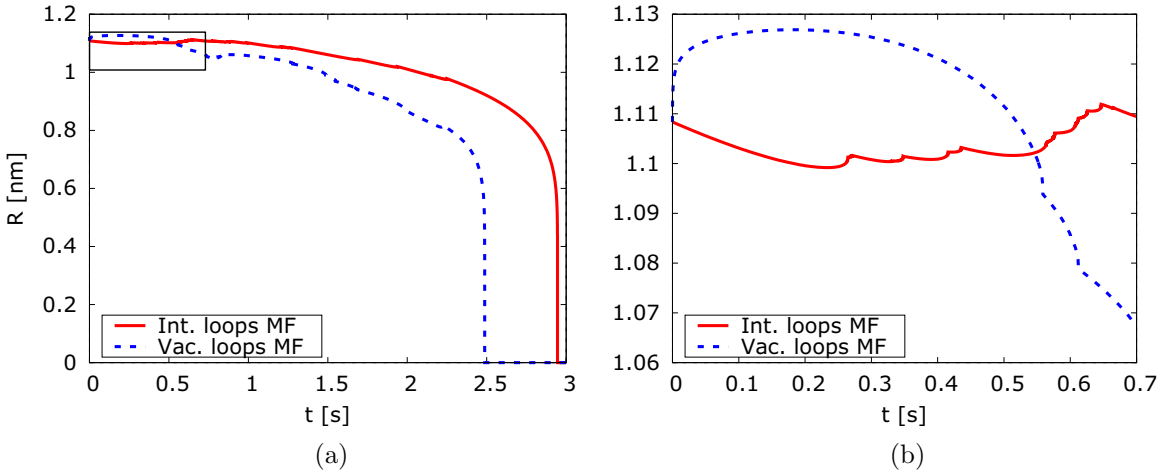

FIG. 11. Same as Fig. 10 but for a cavity number density of 10^{-5} nm^{-3}. The cavity is located at $z = 0.65H$.

metals might be extremely mobile, with collective diffusion coefficients comparable to single interstitials. Therefore, it would be useful to incorporate the mobility of dislocation loops in the model. The introduction of elastic interactions between dislocation loops, cavities, and surfaces would also be a valuable addition, because they have been shown to

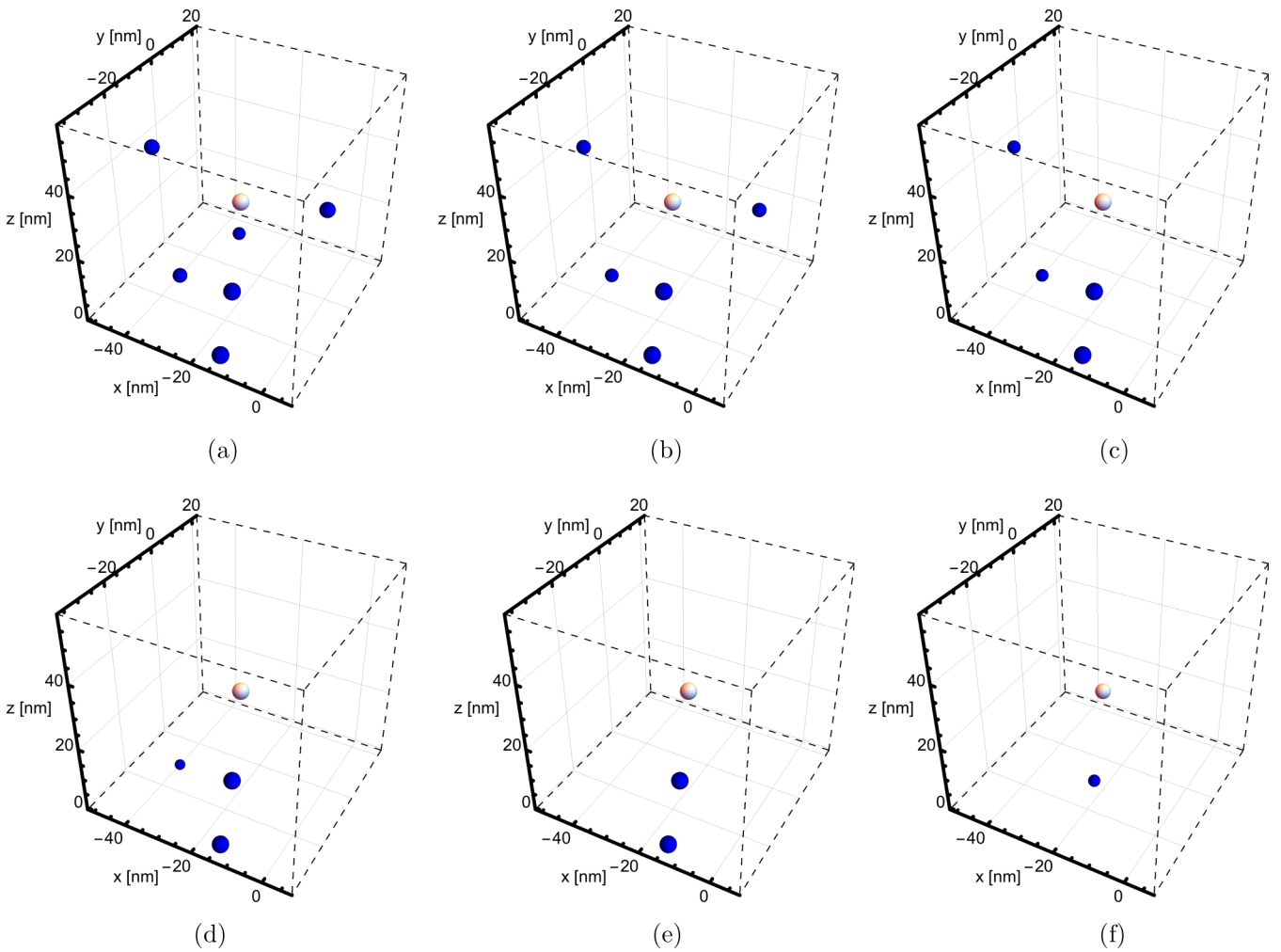

FIG. 12. Snapshots of the evolution of the cavity of Fig. 11, shaded in orange and white in the cell center, and neighboring cavities in blue; (a) initial configuration, (b) $t = 0.208$ s, (c) $t = 0.435$ s, (d) $t = 0.586$ s, (e) $t = 0.632$ s, (f) $t = 2.05$ s. The plots show only a small portion of the periodic cell. The sizes of the cavities have been increased by a factor of 2 for greater clarity.

be a critical factor in determining the large scale spatial distribution of dislocation loops [50]. Additionally, elastic interactions between large numbers of dislocation loops are also responsible for partially suppressing their one-dimensional diffusion, as loops may to be confined in local minima of interaction energy.

In this work we assumed the mobile point defects are exclusively monovacancies. It is possible to adapt the model to the case of interstitial-only diffusion with relative ease. Doing so would generate similar dynamics, with a perfectly symmetrical inversion between the behavior of interstitial and vacancy loops, while cavities would evolve at a considerably reduced rate. It would be more involved to treat *both* monovacancies and single interstitials as diffusing species, since it would require the introduction of reaction rates for the annihilation of the two species in the bulk. It would also be necessary to introduce bias factors between cluster-vacancy and cluster-interstitial interactions because the evolution of the cluster would no longer be determined by a unique point-defect absorption or emission mechanism.

ACKNOWLEDGMENTS

This work has been carried out within the framework of the EUROfusion Consortium and has received funding from the Euratom Research and Training Programme 2014–2018 under Grant Agreement No. 633053. Also, it has been partially funded by the RCUK Energy Programme (Grant No. EP/P012450/1). The views and opinions expressed herein do not necessarily reflect those of the European Commission. I.R. was also supported by the EPSRC Centre for Doctoral Training on Theory and Simulation of Materials at Imperial College London under Grant No. EP/L015579/1. A.P.S. is grateful to the Blackett Laboratory for the provision of laboratory facilities.

APPENDIX A: RELAXATION VOLUME OF A DISLOCATION LOOP AND ITS EVOLUTION IN TIME

Let us consider an arbitrarily shaped dislocation loop, not necessarily planar, with Burgers vector $\mathbf{b}$ and bounded by a piecewise linear dislocation line Γ divided in N segments. Given an arbitrary orthogonal coordinate system, let $\mathbf{R}_i$ and $\mathbf{R}_{i+1} = \mathbf{R}_i + \Delta\mathbf{L}_i$ be the vectors denoting the extremes of the ith segment on Γ, with $\Delta\mathbf{L}_i$ parallel to the dislocation line direction, and $\mathbf{R}_{N+1} = \mathbf{R}_1$. The vector area of the triangle identified by the origin $\mathbf{O}$, $\mathbf{R}_i$, and $\mathbf{R}_{i+1}$ is given by

$$\mathbf{A}_i = \tfrac{1}{2}(\mathbf{R}_i \times \mathbf{R}_{i+1}). \tag{A1}$$

Summing the individual contributions given by the N triangles, we obtain the total vector area of the loop:

$$\mathbf{A} = \sum_{i=1}^{N} \mathbf{A}_i = \frac{1}{2}\sum_{i=1}^{N} (\mathbf{R}_i \times \mathbf{R}_{i+1}), \tag{A2}$$

which, in order to be a well-defined quantity, has to be independent from the choice of the origin of coordinates. In order to prove this statement, let us shift the coordinate system by an arbitrary vector $\mathbf{R}_0$ and compute the new $\mathbf{A}'$:

$$\begin{aligned}\mathbf{A}' &= \frac{1}{2}\sum_{i=1}^{N}[(\mathbf{R}_i + \mathbf{R}_0) \times (\mathbf{R}_{i+1} + \mathbf{R}_0)] \\ &= \frac{1}{2}\sum_{i=1}^{N}(\mathbf{R}_i \times \mathbf{R}_{i+1}) + \frac{1}{2}\mathbf{R}_0 \times \underbrace{\sum_{i=1}^{N}(\mathbf{R}_{i+1} - \mathbf{R}_i)}_{0} = \mathbf{A}.\end{aligned} \tag{A3}$$

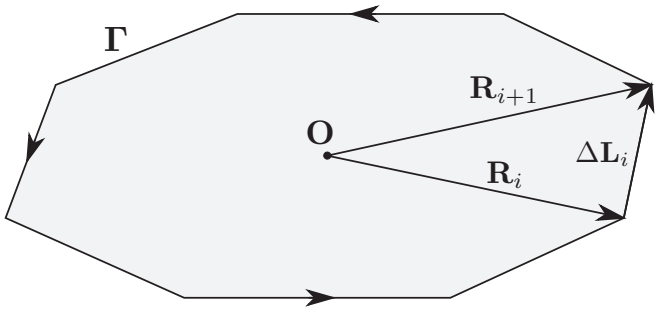

FIG. 13. Sketch of the vectors $\mathbf{R}_i$, $\mathbf{R}_{i+1}$, and $\Delta\mathbf{L}_i$ with respect to the boundary Γ of the dislocation loop. The arrows on Γ denote the direction of the dislocation line.

Therefore $\mathbf{A}$ is indeed a well-defined measure for the vector area of a dislocation loop. A formula for the vector area of a dislocation loop can also be written in the form of a contour integral, see Eq. (27.11) of Ref. [41], as

$$\mathbf{A} = \frac{1}{2}\oint (\mathbf{x} \times d\mathbf{l}), \tag{A4}$$

where $\mathbf{x} \in \Gamma$ and $d\mathbf{l}$ is everywhere tangential to the dislocation line. In the notations of Fig. 13 the above equation corresponds to the limit $N \to \infty$.

Using the convention for the Burgers vector and the dislocation line tangential vector adopted in [33], we now define the relaxation volume of the loop as follows:

$$\mathcal{V} = -(\mathbf{b} \cdot \mathbf{A}) = -\frac{1}{2}\mathbf{b} \cdot \sum_{i=1}^{N}(\mathbf{R}_i \times \mathbf{R}_{i+1}), \tag{A5}$$

which is correctly negative for vacancy prismatic loops, where $\mathbf{b}$ is parallel to $\mathbf{A}$, and positive for interstitial prismatic loops, where $\mathbf{b}$ is antiparallel to $\mathbf{A}$. We now consider the continuous limit for $|\Delta\mathbf{L}_i| \to 0$ and $N \to \infty$, leading to the line integral:

$$\mathcal{V} = -\frac{1}{2}\oint_{\Gamma} \mathbf{b} \cdot (\mathbf{x} \times d\mathbf{l}). \tag{A6}$$

Let us assume that the line Γ, defining the perimeter of the dislocation loop, is parametrized by variable $\varphi \in [0, 1)$ and that it evolves with time, so that for $\mathbf{x} \in \Gamma$ we have $\mathbf{x} = \mathbf{x}(\varphi, t)$ and $d\mathbf{l} = \frac{\partial \mathbf{x}}{\partial \varphi} d\varphi$. We can then write $\mathcal{V}$(t) as

$$\mathcal{V}(t) = -\frac{1}{2}\mathbf{b} \cdot \int_0^1 \left[\mathbf{x}(\varphi, t) \times \frac{\partial \mathbf{x}}{\partial \varphi}(\varphi, t)\right] d\varphi \tag{A7}$$

and its temporal rate of change as

$$\frac{d\mathcal{V}}{dt} = -\frac{1}{2}\mathbf{b}\cdot\left\{\int_0^1\left[\frac{d\mathbf{x}}{dt}\times\frac{\partial\mathbf{x}}{\partial\varphi}\right]d\varphi + \int_0^1\left[\mathbf{x}\times\frac{\partial}{\partial\varphi}\left(\frac{d\mathbf{x}}{dt}\right)\right]d\varphi\right\}. \tag{A8}$$

Using integration by parts, the second integral in the right-hand side can be rearranged as

$$\int_0^1\left[\mathbf{x}\times\frac{\partial}{\partial\varphi}\left(\frac{d\mathbf{x}}{dt}\right)\right]d\varphi = \underbrace{\left[\mathbf{x}\times\frac{d\mathbf{x}}{dt}\right]\Big|_{\varphi=0}^{\varphi=1}}_{0} - \int_0^1\left[\frac{\partial\mathbf{x}}{\partial\varphi}\times\frac{d\mathbf{x}}{dt}\right]d\varphi = \int_0^1\left[\frac{d\mathbf{x}}{dt}\times\frac{\partial\mathbf{x}}{\partial\varphi}\right]d\varphi \tag{A9}$$

so that

$$\frac{d\mathcal{V}}{dt} = -\mathbf{b}\cdot\int_0^1\left[\frac{d\mathbf{x}}{dt}\times\frac{\partial\mathbf{x}}{\partial\varphi}\right]d\varphi = -\oint_\Gamma\mathbf{b}\cdot\left[\frac{d\mathbf{x}}{dt}\times d\mathbf{l}\right], \tag{A10}$$

which is a slightly modified form of Eqs. (4)–(2) (where it was given without proof) found in [33]. We can recast Eq. (A10) in a form more convenient for our applications:

$$\frac{d\mathcal{V}}{dt} = -\oint_\Gamma\mathbf{b}\cdot\left(\frac{d\mathbf{x}}{dt}\times d\mathbf{l}\right) = -\oint_\Gamma\mathbf{b}\cdot(\mathbf{v}\times d\mathbf{l}) = -\oint_\Gamma\mathbf{v}(\mathbf{x})\cdot(d\mathbf{l}\times\mathbf{b}) = -\oint_\Gamma v_{\rm cl}(\mathbf{x})b_e(\mathbf{x})dl, \tag{A11}$$

where $\mathbf{v}(\mathbf{x}) = d\mathbf{x}/dt$ is the vector velocity of a point $\mathbf{x}\in\Gamma$, $v_{\rm cl}$ is the (scalar) dislocation climb velocity, b_e is the edge component of the Burgers vector, and dl is the differential arc length on Γ.

APPENDIX B: PERTURBATIVE EXPANSION OF THE FORMAL SCATTERING SERIES

Let us combine Eqs. (22) and (23) in order to obtain a formal scattering series for the concentration field:

$$\begin{aligned} c(\mathbf{x};\mathcal{X},\mathcal{R}) = c_b(\mathbf{x}) &+ \sum_{i=1}^n \xi_\Delta(R_i)G(\mathbf{x},\mathbf{x}_i)[c_b(\mathbf{x}_i) - c_\Delta(R_i)] \\ &+ \sum_{i=1}^n\sum_{j\neq i} G(\mathbf{x},\mathbf{x}_i)\xi_\Delta(R_i)G(\mathbf{x}_i,\mathbf{x}_j)\xi_\Delta(R_j)[c_b(\mathbf{x}_j) - c_\Delta(R_j)] \\ &+ \sum_{i=1}^n\sum_{j\neq i}\sum_{k\neq j} G(\mathbf{x},\mathbf{x}_i)\xi_\Delta(R_i)G(\mathbf{x}_i,\mathbf{x}_j)\xi_\Delta(R_j)G(\mathbf{x}_j,\mathbf{x}_k)\xi_\Delta(R_k)[c_b(\mathbf{x}_k) - c_\Delta(R_k)] + \cdots \end{aligned} \tag{B1}$$

We can now recast Eq. (B1) in a manner similar to classical scattering theory:

$$\begin{aligned} c(\mathbf{x};\mathcal{X},\mathcal{R}) = c_b(\mathbf{x}) &+ \sum_{i=1}^n\int d\mathbf{x}'d\mathbf{x}''dR\; G(\mathbf{x},\mathbf{x}')\mathcal{T}_i(\mathbf{x}',\mathbf{x}'',R)[c_b(\mathbf{x}'') - c_\Delta(R)] \\ &+ \sum_{i=1}^n\sum_{j\neq i}\int d\mathbf{x}'d\mathbf{x}''d\mathbf{x}'''d\mathbf{x}^{iv}dRdR'G(\mathbf{x},\mathbf{x}')\mathcal{T}_i(\mathbf{x}',\mathbf{x}'',R)G(\mathbf{x}'',\mathbf{x}''')\mathcal{T}_j(\mathbf{x}''',\mathbf{x}^{iv},R')[c_b(\mathbf{x}^{iv}) - c_\Delta(R')] + \cdots, \end{aligned} \tag{B2}$$

where $\mathcal{T}$ is a scattering operator defined by

$$\mathcal{T}_i(\mathbf{x},\mathbf{x}',R) = \xi_\Delta(R)\delta(\mathbf{x}-\mathbf{x}_i)\delta(\mathbf{x}'-\mathbf{x}_i)\delta(R-R_i). \tag{B3}$$

Equivalently, in momentum space, using the Fourier transform definition $f(\mathbf{x}) = (2\pi)^{-3/2}\int d\mathbf{q}e^{i\mathbf{q}\cdot\mathbf{x}}\tilde{f}(\mathbf{q})$, we have

$$\begin{aligned} \tilde{c}(\mathbf{q};\mathcal{X},\mathcal{R}) = \tilde{c}_b(\mathbf{q}) &+ \sum_{i=1}^n\int đ\mathbf{q}'dR\;\tilde{G}(\mathbf{q})\tilde{\mathcal{T}}_i(\mathbf{q}-\mathbf{q}',R)[\tilde{c}_b(\mathbf{q}') - (2\pi)^{3/2}\delta(\mathbf{q}')c_\Delta(R)] \\ &+ \sum_{i=1}^n\sum_{j\neq i}\int đ\mathbf{q}'\mathbf{q}''dRdR'\tilde{G}(\mathbf{q})\tilde{\mathcal{T}}_i(\mathbf{q}-q',R)\tilde{G}(\mathbf{q}')\tilde{\mathcal{T}}_j(\mathbf{q}'-\mathbf{q}'',R')[[\tilde{c}_b(\mathbf{q}'') - (2\pi)^{3/2}\delta(\mathbf{q}'')c_\Delta(R')] + \cdots, \end{aligned} \tag{B4}$$

where

$$\tilde{\mathcal{T}}_i(\mathbf{q},R) = \xi_\Delta(R)\delta(R-R_i)e^{-i\mathbf{q}\cdot\mathbf{x}_i} \tag{B5}$$

and $đ\mathbf{q} = (2\pi)^{-3/2}d\mathbf{q}$.

We can similarly write a corresponding equation for the configuration-averaged concentration:

$$\begin{aligned}\bar{c}(\mathbf{x}) &= c_b(\mathbf{x}) + \int d\mathbf{x}' d\mathbf{x}'' dR\; G(\mathbf{x},\mathbf{x}')\mathcal{S}(\mathbf{x}',\mathbf{x}'',R)[\bar{c}(\mathbf{x}'') - c_\Delta(R)] \\ &= c_b(\mathbf{x}) + \int d\mathbf{x}' d\mathbf{x}'' dR\; G(\mathbf{x},\mathbf{x}')\mathcal{S}(\mathbf{x}',\mathbf{x}'',R)[c_b(\mathbf{x}'') - c_\Delta(R)] \\ &\quad + \int d\mathbf{x}' d\mathbf{x}'' d\mathbf{x}''' d\mathbf{x}^{iv} dR dR' G(\mathbf{x},\mathbf{x}')\mathcal{S}(\mathbf{x}',\mathbf{x}'',R)G(\mathbf{x}'',\mathbf{x}''')\mathcal{S}(\mathbf{x}''',\mathbf{x}^{iv},R')[c_b(\mathbf{x}^{iv}) - c_\Delta(R')] + \cdots, \end{aligned} \tag{B6}$$

which also serves as a definition for the "self-energy" $\mathcal{S}$, physically representing the interaction of the mean field with itself. An analogous equation in momentum space takes the form

$$\begin{aligned}\tilde{\bar{c}}(\mathbf{q}) &= \tilde{c}_b(\mathbf{q}) + \int dR\; \tilde{G}(\mathbf{q})\tilde{\mathcal{S}}(\mathbf{q},R)[\tilde{\bar{c}}(\mathbf{q}') - (2\pi)^{3/2}\delta(\mathbf{q}')c_\Delta(R)] \\ &= \tilde{c}_b(\mathbf{q}) + \int dR\; \tilde{G}(\mathbf{q})\tilde{\mathcal{S}}(\mathbf{q},R)[\tilde{c}_b(\mathbf{q}') - (2\pi)^{3/2}\delta(\mathbf{q}')c_\Delta(R)] \\ &\quad + \int dR dR' \tilde{G}(\mathbf{q})\tilde{\mathcal{S}}(\mathbf{q},R)\tilde{G}(\mathbf{q})\tilde{\mathcal{S}}(\mathbf{q},R')[\tilde{c}_b(\mathbf{q}') - (2\pi)^{3/2}\delta(\mathbf{q}')c_\Delta(R)] + \cdots. \end{aligned} \tag{B7}$$

In order to determine the function $\tilde{\mathcal{S}}(\mathbf{q},R)$ we now have to perform the configuration average in terms of the scattering operators $\tilde{\mathcal{T}}_i(\mathbf{q},R)$, and compare the resulting expression with Eq. (B7), using an approach similar to the one implemented by Marqusee and Ross [21].

By introducing the notation $\overline{f} = \int f(\mathcal{X},\mathcal{R})p(\mathcal{X},\mathcal{R})d\mathcal{X}d\mathcal{R}$, the configuration average of Eq. (B4) takes the form

$$\begin{aligned}\tilde{\bar{c}}(\mathbf{q}) &= \tilde{c}_b(\mathbf{q}) + \sum_{i=1}^{n}\int đ\mathbf{q}' dR\; \tilde{G}(\mathbf{q})\overline{\tilde{\mathcal{T}}_i(\mathbf{q}-\mathbf{q}',R)}[\tilde{c}_b(\mathbf{q}') - (2\pi)^{3/2}\delta(\mathbf{q}')c_\Delta(R)] \\ &\quad + \sum_{i=1}^{n}\sum_{j\neq i}\int đ\mathbf{q}' đ\mathbf{q}'' dR dR' \tilde{G}(\mathbf{q})\overline{\tilde{\mathcal{T}}_i(\mathbf{q}-\mathbf{q}',R)\tilde{G}(\mathbf{q}')\tilde{\mathcal{T}}_j(\mathbf{q}'-\mathbf{q}'',R')}[[\tilde{c}_b(\mathbf{q}'') - (2\pi)^{3/2}\delta(\mathbf{q}'')c_\Delta(R')] + \cdots. \end{aligned} \tag{B8}$$

Let us define $\tilde{\mathcal{S}}_j(\mathbf{q},R)$ as the contribution to $\tilde{\mathcal{S}}$ containing the product of exactly a number j of $\tilde{\mathcal{T}}$ operators, i.e., $\tilde{\mathcal{S}} = \sum_j^\infty \tilde{\mathcal{S}}_j$.

By comparing Eqs. (B7) and (B8) we can determine each order of the self-energy recursively:

$$\begin{aligned}\tilde{\mathcal{S}}_1(\mathbf{q},R) &= \sum_{i=1}^{n}\int đ\mathbf{q}'\overline{\tilde{\mathcal{T}}_i(\mathbf{q}-\mathbf{q}',R)}, \\ \tilde{\mathcal{S}}_2(\mathbf{q},R) &= \int đ\mathbf{q}'' đ\mathbf{q}'' dR' \sum_{i=1}^{n}\sum_{j\neq i}\overline{\tilde{\mathcal{T}}_i(\mathbf{q}-\mathbf{q}',R')\tilde{G}(\mathbf{q}')\tilde{\mathcal{T}}_j(\mathbf{q}'-\mathbf{q}'',R)} - \int dR'\tilde{\mathcal{S}}_1(\mathbf{q},R')\tilde{G}(\mathbf{q})\tilde{\mathcal{S}}_1(\mathbf{q},R), \\ \tilde{\mathcal{S}}_3(\mathbf{q},R) &= \int đ\mathbf{q}' đ\mathbf{q}'' đ\mathbf{q}''' dR' dR'' \sum_{i=1}^{n}\sum_{j\neq i}\sum_{k\neq j}\overline{\tilde{\mathcal{T}}_i(\mathbf{q}-\mathbf{q}',R'')\tilde{G}(\mathbf{q}')\tilde{\mathcal{T}}_j(\mathbf{q}'-\mathbf{q}'',R'')\tilde{G}(\mathbf{q}'')\tilde{\mathcal{T}}_k(\mathbf{q}''-\mathbf{q}''',R)} \\ &\quad - \int dR' dR''\tilde{\mathcal{S}}_1(\mathbf{q},R'')\tilde{G}(\mathbf{q})\tilde{\mathcal{S}}_1(\mathbf{q},R')\tilde{G}(\mathbf{q})\tilde{\mathcal{S}}_1(\mathbf{q},R) \\ &\quad - \int dR'[\tilde{\mathcal{S}}_1(\mathbf{q},R')\tilde{G}(\mathbf{q})\tilde{\mathcal{S}}_2(\mathbf{q},R) + \tilde{\mathcal{S}}_2(\mathbf{q},R')\tilde{G}(\mathbf{q})\tilde{\mathcal{S}}_1(\mathbf{q},R)] \end{aligned} \tag{B9}$$

and so on.

The general pattern is evident: $\tilde{\mathcal{S}}_n$ contains a term of the form $\overline{\tilde{\mathcal{T}}\tilde{G}\tilde{\mathcal{T}}\tilde{G}\tilde{\mathcal{T}}\ldots}$, with respectively n and $n-1$ $\tilde{\mathcal{T}}$ and $\tilde{G}$ operators, minus all the possible unique combinations of lower order $\tilde{\mathcal{S}}$ and $\tilde{G}$ terms containing exactly a number n of $\tilde{\mathcal{T}}$ operators. Let us assume that the loops are homogeneously distributed in space and that there are no correlations either in the positions or radii of different loops, allowing us to write

$$p_1(\mathbf{x},R) = n^{-1}f(R), \tag{B10}$$

where $f(R)dR$ is the number density of dislocation loops with radii in the range $(R, R+dR)$. We also consider the thermodynamic limit of $n\to\infty$, with constant number density. The first contributions to $\mathcal{S}$ can then be explicitly expressed as

$$\tilde{\mathcal{S}}_1(\mathbf{q},R) = \xi_\Delta(R)f(R), \quad \tilde{\mathcal{S}}_2(\mathbf{q},R) = -\overline{\xi_\Delta}\tilde{G}(\mathbf{q})\xi_\Delta(R)f(R), \quad \tilde{\mathcal{S}}_3(\mathbf{q},R) = \overline{\xi_\Delta}\xi_\Delta^2(R)f(R)\int đ\mathbf{q}''\tilde{G}^2(\mathbf{q}). \tag{B11}$$

APPENDIX C: EWALD SUMMATION OF THE DIFFUSIVE INTERACTIONS IN A THIN FILM GEOMETRY

Consider a periodic system in three dimensions with N clusters with effective charges $\{Q_i\}_{i=1}^N$ and N "image" clusters with effective charges $\{-Q_i\}_{i=1}^N$ per primitive cell. The primitive cell is defined as $\Gamma(0) = \{\mathbf{x} = x_1\mathbf{a}_1 + x_2\mathbf{a}_2 + x_3\mathbf{a}_3 : -1/2 < x_\alpha < 1/2, \alpha = 1, 2, 3\}$, with primitive vectors $\mathbf{a}_1 = (L, 0, 0)$, $\mathbf{a}_2 = (0, L, 0)$, and $\mathbf{a}_3 = (0, 0, 2H)$.

Let $\mathbf{m} = m_1\mathbf{a}_1 + m_2\mathbf{a}_2 + m_3\mathbf{a}_3$, $m_\alpha \in \mathbb{Z}$, and $\bar{\mathbf{x}}_j = (x_j, y_j, \mathrm{sgn}(z_j)H - z_j)$ and $G_Y(\mathbf{x}, \mathbf{x}'; \overline{\xi_\Delta}) = -e^{-\sqrt{\overline{\xi_\Delta}/D_v}}(4\pi D_v|\mathbf{x} - \mathbf{x}'|)^{-1}$. We want to reformulate the expression

$$K(\mathbf{x}_i, \mathbf{x}_j, \overline{\xi_\Delta}) = {\sum_{\mathbf{m}}}' G_Y(\mathbf{x}_i, \mathbf{m} + \mathbf{x}_j; \overline{\xi_\Delta}) - \sum_{\mathbf{m}} G_Y(\mathbf{x}_i, \mathbf{m} + \bar{\mathbf{x}}_j; \overline{\xi_\Delta}) \qquad i = 1, \ldots, N \tag{C1}$$

as an absolutely convergent series in real and reciprocal space.

We first define a "primitive cell effective Green's function" as follows:

$$G_Y^\Gamma(\mathbf{x}; \overline{\xi_\Delta}) = \sum_{\mathbf{m}} G_Y(\mathbf{x} + \mathbf{m}; \overline{\xi_\Delta}), \tag{C2}$$

which satisfies the equation

$$(D_v\nabla^2 - \overline{\xi_\Delta})G_Y^\Gamma(\mathbf{x}; \overline{\xi_\Delta}) = \delta^\Gamma(\mathbf{x}) = \sum_{\mathbf{m}} \delta(\mathbf{x} + \mathbf{m}). \tag{C3}$$

We split the primitive cell Green's function: $G_Y^\Gamma = G_{Y,F}^\Gamma + G_{Y,D}^\Gamma$, where

$$\begin{aligned}(D_v\nabla^2 - \overline{\xi_\Delta})G_{Y,F}^\Gamma(\mathbf{x}; \overline{\xi_\Delta}) &= \sum_{\mathbf{m}} \lambda\rho_\beta(\mathbf{x} + \mathbf{m}),\\ (D_v\nabla^2 - \overline{\xi_\Delta})G_{Y,D}^\Gamma(\mathbf{x}; \overline{\xi_\Delta}) &= \sum_{\mathbf{m}} [\delta(\mathbf{x} + \mathbf{m}) - \lambda\rho_\beta(\mathbf{x} + \mathbf{m})],\end{aligned} \tag{C4}$$

and $\rho_\beta(\mathbf{x})$ is a normalized Gaussian distribution:

$$\rho_\beta(\mathbf{x}) = \left(\frac{\beta^2}{\pi}\right)^{3/2} e^{-\beta^2|\mathbf{x}|^2}. \tag{C5}$$

Let us introduce a reciprocal lattice with basis vectors: $\mathbf{b}_1 = (1/L, 0, 0)$, $\mathbf{b}_2 = (0, 1/L, 0)$, and $\mathbf{b}_3 = (0, 0, 1/2H)$, and the general reciprocal space vector as $\mathbf{k} = k_1\mathbf{b}_1 + k_2\mathbf{b}_2 + k_3\mathbf{b}_3$, $k_\alpha \in \mathbb{Z}$, $\alpha = 1, 2, 3$. In particular, $G_{Y,F}^\Gamma$ is more conveniently expressed in terms of reciprocal space functions. By Fourier transforming ρ_β and using the relation $\sum_{\mathbf{m}} \delta(\mathbf{x} + \mathbf{m}) = \sum_{\mathbf{k}} \exp(i\mathbf{k} \cdot \mathbf{x})$, we have

$$G_{Y,F}^\Gamma(\mathbf{x}, \overline{\xi_\Delta}) = -\frac{\lambda}{V} \sum_{\mathbf{k}} \frac{\exp(i\mathbf{k} \cdot \mathbf{x} - k^2/4\beta^2)}{D_v k^2 + \overline{\xi_\Delta}}, \tag{C6}$$

where V is the volume of the primitive cell. On the other hand, we have

$$G_{Y,D}^\Gamma(\mathbf{x}; \overline{\xi_\Delta}) = G_Y^\Gamma(\mathbf{x}; \overline{\xi_\Delta}) - G_{Y,F}^\Gamma(\mathbf{x}; \overline{\xi_\Delta}) = \sum_{\mathbf{m}} [G_Y(\mathbf{x} + \mathbf{m}; \overline{\xi_\Delta}) - \lambda\psi_\beta(\mathbf{x} + \mathbf{m})], \tag{C7}$$

where the potential $\psi_\beta(\mathbf{x})$ is given by

$$\begin{aligned}\psi_\beta(\mathbf{x}) = \int d\mathbf{x}' G_Y(\mathbf{x}, \mathbf{x}', \overline{\xi_\Delta})\rho_\beta(\mathbf{x}') = -\frac{e^{\overline{\xi_\Delta}/4D_v\beta^2}}{4\pi D_v} \Bigg\{ \frac{e^{-\sqrt{\overline{\xi_\Delta}/D_v}|\mathbf{x}|}}{2|\mathbf{x}|} \Bigg[\mathrm{erf}\left(\beta|\mathbf{x}| + \frac{\sqrt{\overline{\xi_\Delta}/D_v}}{2\beta}\right)\\ + \mathrm{erf}\left(\beta|\mathbf{x}| - \frac{\sqrt{\overline{\xi_\Delta}/D_v}}{2\beta}\right)\Bigg] - \sinh(\sqrt{\overline{\xi_\Delta}/D_v}|\mathbf{x}|)\mathrm{erfc}\left(\beta|\mathbf{x}| + \frac{\sqrt{\overline{\xi_\Delta}/D_v}}{2\beta}\right)\Bigg\}.\end{aligned} \tag{C8}$$

The parameter λ should be chosen in a way that minimizes the long tail of $G^{\Gamma}_{Y,D}$. In particular, as $|\mathbf{x}| \to \infty$, $\psi_\beta(\mathbf{x}) \simeq \frac{e^{\overline{\xi_\Delta}^2/4\beta^2 - \overline{\xi_\Delta}|\mathbf{x}|}}{|\mathbf{x}|}$, therefore the optimal choice is $\lambda = e^{-\overline{\xi_\Delta}^2/4\beta^2}$ and G^{Γ}_{Y} assumes the form

$$G^{\Gamma}_{Y}(\mathbf{x};\overline{\xi_\Delta}) = -\sum_{\mathbf{k}} \frac{\exp[-(k^2+\overline{\xi_\Delta}/D_v)/4\beta^2]}{V(D_v k^2+\overline{\xi_\Delta})} e^{i\mathbf{k}\cdot\mathbf{x}} - \frac{1}{8\pi D_v}\sum_{\mathbf{m}}\frac{1}{|\mathbf{x}+\mathbf{m}|}\left[\operatorname{erfc}\left(\beta|\mathbf{x}+\mathbf{m}| + \frac{\sqrt{\overline{\xi_\Delta}/D_v}}{2\beta}\right)e^{\sqrt{\overline{\xi_\Delta}/D_v}|\mathbf{x}+\mathbf{m}|}\right.$$
$$\left. + \operatorname{erfc}\left(\beta|\mathbf{x}+\mathbf{m}| - \frac{\sqrt{\overline{\xi_\Delta}/D_v}}{2\beta}\right)e^{-\sqrt{\overline{\xi_\Delta}/D_v}|\mathbf{x}+\mathbf{m}|}\right]. \tag{C9}$$

We now have to remove the spurious self-interactions:

$$\begin{aligned}
\sum_{\mathbf{m}}{}' G_Y(\mathbf{x}_i, \mathbf{m}+\mathbf{x}_i;\overline{\xi_\Delta}) &= \lim_{\mathbf{x}\to\mathbf{x}_i}\left[G^{\Gamma}_{Y}(\mathbf{x},\mathbf{x}_i;\overline{\xi_\Delta}) - G_Y(\mathbf{x},\mathbf{x}_i;\overline{\xi_\Delta})\right] \\
&= -\sum_{\mathbf{k}}\frac{\exp[-(k^2+\overline{\xi_\Delta}/D_v)/4\beta^2]}{V(D_v k^2+\overline{\xi_\Delta})} \\
&\quad - \frac{1}{8\pi D_v}\sum_{\mathbf{m}\neq\mathbf{0}}\frac{1}{|\mathbf{m}|}\left[\operatorname{erfc}\left(\beta|\mathbf{m}| + \frac{\sqrt{\overline{\xi_\Delta}/D_v}}{2\beta}\right)e^{\sqrt{\overline{\xi_\Delta}/D_v}|\mathbf{m}|} + \operatorname{erfc}\left(\beta|\mathbf{m}| - \frac{\sqrt{\overline{\xi_\Delta}/D_v}}{2\beta}\right)e^{-\sqrt{\overline{\xi_\Delta}/D_v}|\mathbf{m}|}\right] \\
&\quad - \frac{1}{4\pi D_v}\lim_{r\to 0}\frac{1}{r}\left[\operatorname{erfc}\left(\beta r + \frac{\sqrt{\overline{\xi_\Delta}/D_v}}{2\beta}\right)\frac{e^{\sqrt{\overline{\xi_\Delta}/D_v}r}}{2} + \operatorname{erfc}\left(\beta r - \frac{\sqrt{\overline{\xi_\Delta}/D_v}}{2\beta}\right)\frac{e^{-\sqrt{\overline{\xi_\Delta}/D_v}r}}{2} - e^{-\sqrt{\overline{\xi_\Delta}/D_v}r}\right].
\end{aligned} \tag{C10}$$

Expanding to first order with respect to r,

$$\begin{aligned}
&\operatorname{erfc}\left(\beta r + \frac{\sqrt{\overline{\xi_\Delta}/D_v}}{2\beta}\right)\frac{e^{\sqrt{\overline{\xi_\Delta}/D_v}r}}{2} + \operatorname{erfc}\left(\beta r - \frac{\sqrt{\overline{\xi_\Delta}/D_v}}{2\beta}\right)\frac{e^{-\sqrt{\overline{\xi_\Delta}/D_v}r}}{2} - e^{-\sqrt{\overline{\xi_\Delta}/D_v}r} \\
&\approx \left[\sqrt{\frac{\overline{\xi_\Delta}}{D_v}}\operatorname{erfc}\left(\frac{\sqrt{\overline{\xi_\Delta}}}{2\sqrt{D_v}\beta}\right) - \frac{2e^{-\frac{\overline{\xi_\Delta}}{4D_v\beta^2}}}{\sqrt{\pi}}\right]r + O(r^2).
\end{aligned} \tag{C11}$$

We can now combine all the terms, yielding to an absolutely convergent series in real and reciprocal space:

$$\begin{aligned}
K(\mathbf{x}_i,\mathbf{x}_j;\epsilon) &= -\sum_{\mathbf{k}}\frac{\exp[-(k^2+\epsilon^2)/4\beta^2]}{V D_v(k^2+\epsilon^2)}e^{i\mathbf{k}\cdot\mathbf{x}_i}[e^{-i\mathbf{k}\cdot\mathbf{x}_j} - e^{-i\mathbf{k}\cdot\bar{\mathbf{x}}_j}] \\
&\quad - \frac{1}{8\pi D_v}\left\{\sum_{\mathbf{m}}{}'\frac{1}{|\mathbf{x}_i-\mathbf{x}_j+\mathbf{m}|}\left[\operatorname{erfc}\left(\beta|\mathbf{x}_i-\mathbf{x}_j+\mathbf{m}| + \frac{\epsilon}{2\beta}\right)e^{\epsilon|\mathbf{x}_i-\mathbf{x}_j+\mathbf{m}|}\right.\right. \\
&\quad \left. + \operatorname{erfc}\left(\beta|\mathbf{x}_i-\mathbf{x}_j+\mathbf{m}| - \frac{\epsilon}{2\beta}\right)e^{-\epsilon|\mathbf{x}_i-\mathbf{x}_j+\mathbf{m}|}\right] \\
&\quad - \sum_{\mathbf{m}}\frac{1}{|\mathbf{x}_i-\bar{\mathbf{x}}_j+\mathbf{m}|}\left[\operatorname{erfc}\left(\beta|\mathbf{x}_i-\bar{\mathbf{x}}_j+\mathbf{m}| + \frac{\epsilon}{2\beta}\right)e^{\epsilon|\mathbf{x}_i-\bar{\mathbf{x}}_j+\mathbf{m}|}\right. \\
&\quad \left.\left. + \operatorname{erfc}\left(\beta|\mathbf{x}_i-\bar{\mathbf{x}}_j+\mathbf{m}| - \frac{\epsilon}{2\beta}\right)e^{-\epsilon|\mathbf{x}_i-\bar{\mathbf{x}}_j+\mathbf{m}|}\right]\right\} + \frac{\delta_{ij}}{4\pi D_v}\left[\frac{2\beta e^{-\frac{\epsilon^2}{4\beta^2}}}{\sqrt{\pi}} - \epsilon\operatorname{erfc}\left(\frac{\epsilon}{2\beta}\right)\right].
\end{aligned} \tag{C12}$$

[1] W. Van Renterghem and I. Uytdenhouwen, J. Nucl. Mater. **477**, 77 (2016).

[2] F. Ferroni, X. Yi, K. Arakawa, S. P. Fitzgerald, P. D. Edmondson, and S. G. Roberts, Acta Mater. **90**, 380 (2015).

[3] K. Fukumoto, M. Iwasaki, and Q. Xu, J. Nucl. Mater. **442**, 360 (2013).

[4] T. Nagasaka, T. Muroga, H. Watanabe, K. Yamasaki, N.-J. Heo, K. Shinozaki, and M. Narui, Mater. Trans. **46**, 498 (2005).

[5] T. S. Byun, J. H. Baek, O. Anderoglu, S. A. Maloy, and M. B. Toloczko, J. Nucl. Mater. **449**, 263 (2014).

[6] A. E. Sand, S. L. Dudarev, and K. Nordlund, Europhys. Lett. **103**, 46003 (2013).

[7] A. E. Sand, K. Nordlund, and S. L. Dudarev, J. Nucl. Mater. **455**, 207 (2014).

[8] A. E. Sand, M. J. Aliaga, M. J. Caturla, and K. Nordlund, Europhys. Lett. **115**, 36001 (2016).

[9] B. D. Wirth, G. R. Odette, D. Maroudas, and G. E. Lucas, J. Nucl. Mater. **276**, 33 (2000).

[10] R. E. Stoller, S. I. Golubov, C. Domain, and C. S. Becquart, J. Nucl. Mater. **382**, 77 (2008).

[11] S. I. Golubov, A. V. Barashev, and R. E. Stoller, *Comprehensive Nuclear Materials* (Elsevier, Amsterdam, 2012), pp. 357–391.

[12] S. I. Golubov, A. M. Ovcharenko, A. V. Barashev, and B. N. Singh, Philos. Mag. A **81**, 643 (2001).

[13] A. F. Voter, *Radiation Effects in Solids* (Springer, Dordrecht, 2007), pp. 1–23.

[14] C. S. Becquart, A. Barbu, J. L. Bocquet, M. J. Caturla, C. Domain, C. C. Fu, S. I. Golubov, M. Hou, L. Malerba, C. J. Ortiz, A. Souidi, and R. E. Stoller, J. Nucl. Mater. **406**, 39 (2010).

[15] I. Rovelli, S. L. Dudarev, and A. P. Sutton, J. Mech. Phys. Solids **103**, 121 (2017).

[16] Y. Gu, Y. Xiang, S. S. Quek, and D. J. Srolovitz, J. Mech. Phys. Solids **83**, 319 (2015).

[17] X. Yi, A. E. Sand, D. R. Mason, M. A. Kirk, S. G. Roberts, K. Nordlund, and S. L. Dudarev, Europhys. Lett. **110**, 36001 (2015).

[18] L. A. Beavan, R. M. Scanlan, and D. N. Seidman, Acta Metall. **19**, 1339 (1971).

[19] C. Liu, L. He, Y. Zhai, B. Tyburska-Püschel, P. M. Voyles, K. Sridharan, D. Morgan, and I. Szlufarska, Acta Mater. **125**, 377 (2017).

[20] S. F. Edwards, Philos. Mag. **3**, 1020 (1958).

[21] J. A. Marqusee, J. Chem. Phys. **81**, 976 (1984).

[22] V. E. Fradkov, M. E. Glicksman, and S. P. Marsh, Phys. Rev. E **53**, 3925 (1996).

[23] H. Mandyam, M. E. Glicksman, J. Helsing, and S. P. Marsh, Phys. Rev. E **58**, 2119 (1998).

[24] K. G. Wang, M. E. Glicksman, and K. Rajan, Phys. Rev. E **69**, 061507 (2004).

[25] K. G. Wang, Physica A **387**, 3084 (2008).

[26] K. G. Wang and G. Q. Wang, Phys. Rev. E **95**, 022609 (2017).

[27] G. Salin and J. M. Caillol, J. Chem. Phys. **113**, 10459 (2000).

[28] J. Lothe, J. Appl. Phys. **31**, 1077 (1960).

[29] M. J. Turunen, Acta Metall. **24**, 463 (1976).

[30] D. Mordehai, E. Clouet, M. Fivel, and M. Verdier, Philos. Mag. **88**, 899 (2008).

[31] B. Bakó, E. Clouet, L. Dupuy, and M. Blétry, Philos. Mag. **91**, 3173 (2011).

[32] S. Jiang, M. Rachh, and Y. Xiang, Multiscale Model. Simul. **15**, 235 (2017).

[33] J. P. Hirth and J. Lothe, *Theory of Dislocations*, 2nd ed. (Wiley, New York, 1982).

[34] L. Vitos, A. V. Ruban, H. L. Skriver, and J. Kollár, Surf. Sci. **411**, 186 (1998).

[35] G. W. C. Kaye and T. H. Laby, *Tables of Physical and Chemical Constants*, 16th ed. (Longman, Harlow, 1995).

[36] S. L. Dudarev, Annu. Rev. Mater. Res. **43**, 35 (2013).

[37] J. N. Mundy, S. J. Rothman, N. Q. Lam, H. A. Hoff, and L. J. Nowicki, Phys. Rev. B **18**, 6566 (1978).

[38] Y. Iijima, K. Kimura, and K. Hirano, Acta Metall. **36**, 2811 (1988).

[39] J. M. Dupouy, J. Mathie, and Y. Adda, Mem. Sci. Rev. Metall. **63**, 481 (1966).

[40] A. Glensk, B. Grabowski, T. Hickel, and J. Neugebauer, Phys. Rev. X **4**, 011018 (2014).

[41] L. D. Landau and E. M. Lifshitz, *Theory of Elasticity*, 2nd ed. (Pergamon, Oxford, UK, 1970).

[42] H. Trinkaus, Phys. Status Solidi B **54**, 209 (1972).

[43] S. L. Dudarev, Phys. Rev. B **62**, 9325 (2000).

[44] M. R. Gilbert, S. L. Dudarev, P. M. Derlet, and D. G. Pettifor, J. Phys.: Condens. Matter **20**, 345214 (2008).

[45] R. Alexander, M.-C. Marinica, L. Proville, F. Willaime, K. Arakawa, M. R. Gilbert, and S. L. Dudarev, Phys. Rev. B **94**, 024103 (2016).

[46] S. L. Dudarev, A. A. Semenov, and C. H. Woo, Phys. Rev. B **70**, 094115 (2004).

[47] X. Yi, M. L. Jenkins, M. Briceno, S. G. Roberts, Z. Zhou, and M. A. Kirk, Philos. Mag. **93**, 1715 (2013).

[48] K. Arakawa, K. Ono, M. Isshiki, K. Mimura, M. Uchikoshi, and H. Mori, Science **318**, 956 (2007).

[49] P. M. Derlet, M. R. Gilbert, and S. L. Dudarev, Phys. Rev. B **84**, 134109 (2011).

[50] S. L. Dudarev, K. Arakawa, X. Yi, Z. Yao, M. L. Jenkins, M. R. Gilbert, and P. M. Derlet, J. Nucl. Mater. **455**, 16 (2014).